MASTER THESIS

Two-Species Quantum Dimer Models on the Triangular Lattice

Author:
Brin VERHEIJDEN

Supervisor:
Prof. Dr. Matthias PUNK

*A thesis submitted in fulfillment of the requirements
for the degree of Master of Science*

in the

Theoretical Solid State Physics
Theoretische und Mathematische Physik

January 30, 2019

LUDWIGS-MAXIMILLIANS-UNIVERSITÄT, MÜNCHEN

Abstract

Fakultät der Physik
Theoretische und Mathematische Physik

Master of Science

Two-Species Quantum Dimer Models on the Triangular Lattice

by Brin VERHEIJDEN

This thesis introduces a two-dimer model on the triangular lattice which is believed to explain the pseuso-gap phase[1]. An exact expression for the classical Bosonic single-dimer correlation on the triangular lattice is found using Grassman variables, which can be used to find all classical many-dimer correlations. Using said classical correlations, an exact triangular two-dimer ground state[2] is found for a Fermionic extension to the Rokhsar-Kivelson Hamiltonian [3] at the RK-point. This ground state will be perturbed analytically up to first order and investigated. A numerical method is set up, using the Lanczos algorithm, to find the corresponding ground state dispersion for the aforementioned Hamiltonian and perturbations to it. Finally, a suggestion is made for analytical and for numerical validation of the results presented.

---

[1]Punk, Allais, and Sachdev, 2015, Sachdev and Chowdhury, 2016
[2]Feldmeier, Huber, and Punk, 2018
[3]Rokhsar and Kivelson, 1988

Acknowledgements

I would like to thank my supervisor, Matthias Punk, for his support, patience and his vast knowledge of the subject throughout the entirety of the project, whenever I needed it.

A word of gratitude to Sebastian Huber, as well, who helped me make sense of my work by helping me answer many unannounced questions about my analytical work.

One who cannot be left out when displaying my gratitude is my predecessor, Johannes Feldmeier, who's work on the exact ground states for the square lattice formed a comprehensive guide on how to approach these calculations.

Contents

Chapter 1

Introduction to the Dimer Model

1.1 Background

1.1.1 Wannier- and Bloch Functions

When describing electrons on a lattice, the usual approach is to look at each given site is occupied by an electron or not. These occupations are represented by Wannier functions $\{\Psi_{Wannier,x,\sigma}\}$, the position-based counterparts of the momentum-based Bloch functions $\{\Psi_{Bloch,k,\sigma}\}$. Wannier functions have the unique property that they are periodic in (pseuso-)momentum space, as where Bloch functions are periodic in (physical) space. Both the set of Wannier functions and the set of Bloch functions form orthonormal bases for the state space of the corresponding lattice. Working with these functions is usually done in the operator basis (or canonical quantisation). The usual rule for anti-commuting variable can be used, as is typical for Fermionic particles:

$$\{c_{x\sigma}, c^{\dagger}_{x'\sigma'}\} = \delta_{xx',\sigma\sigma'} \tag{1.1}$$

$$\{c_{x\sigma}, c_{x'\sigma'}\} = 0 \tag{1.2}$$

$$\{c^{\dagger}_{x\sigma}, c^{\dagger}_{x'\sigma'}\} = 0 \tag{1.3}$$

$$c_{x\sigma}|0\rangle = 0 \tag{1.4}$$

Where $|0\rangle$ is the ground state. Equations 1.1 to 1.4 analogously for $c_{k\sigma}$ and $c^{\dagger}_{k\sigma}$. Finally, the Wannier states and Bloch states are related to each other via equation 1.5, where N is the total number of lattice sites.

$$c_{x\sigma} = \frac{1}{\sqrt{N}} \sum_k e^{ikx} c_{k\sigma} \tag{1.5}$$

This description in terms single electrons allows one to mathematically set up electron-electron interactions in a very controlled way. The corresponding Hilbert space is well defined, and it scales with the number of sites as 4^N. This because each site can have four different states ($|0\rangle$, $|\uparrow\rangle$, $|\downarrow\rangle$ and $|\uparrow\downarrow\rangle$). It works well ($N^{th}$-)nearest neighbour interactions and momentum exchange between, to name a few examples.

1.1.2 Hubbard Model

When using the operator basis, the simplest model that can be studied with interactions is the Hubbard model. This model consists of a hopping term J and a potential term U, as shown in equation 1.6.

$$H = -J \sum_{\langle i,j \rangle, \sigma} c_{i\sigma}^{\dagger} c_{j\sigma} + U \sum_{i} c_{i\uparrow}^{\dagger} c_{i\uparrow} c_{i\downarrow}^{\dagger} c_{i\downarrow} \tag{1.6}$$

The indices in brackets are nearest neighbours (defined in terms of physical distance). Even though this model is quite simple, much of it is not yet understood. The interesting part for this thesis is when the potential is dominating $|U| \gg |J|$. For a strongly attractive potential (U negative) there is a very strong pairing of pairs of opposite spin on each site, but in the case of a repulsive (positive) U, the system becomes Mott-insulating. This is a unique and anti-ferromagnetic state with highly suppressed fluctuations. This Mott state can only exist at (and very close) half-filling (a single Fermion per site). When the state deviates from this near-perfect half filling, the state stays anti-ferromagnetic, though what exactly happens is not entirely figured out yet.
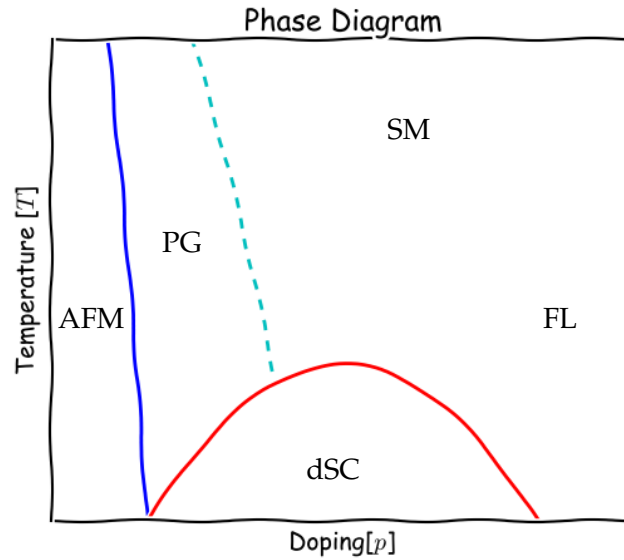
FIGURE 1.1: This figure shows the phase diagram of the Fermi-Hubbard model as function of temperature and hole doping. Showing the following phases: antiferromagnet (AFM), d-wave superconductor (dSC), Fermi-liquid (FL), strange metal (SM) and pseudo-gap metal (PG).

Figure 1.1 shows a phase diagram in terms of the hole doping p and temperature T, that is experimentally found and expected to be the result of the Hubbard model near half-filling[1]. It shows the anti-ferromagnetic (AFM) state near $p = 0$ (p positive means less electrons), which becomes a Mott insulator at high temperatures, close to $p = 0$. The red phase is a d-wave superconductor (dSC) and further it shows what is known as a strange metal phase (SM), the metallic Fermi liquid phase (FL) and the pseudo-gap metal (PG). This last phase is what this thesis is trying to explain.

The pseudo-gap phase is an anti-ferromagnetic metallic state. Where for a Fermi liquid, the charge carrier density n is something that goes with the hole density: $n = 1 + p$ (half-filling + doping), the pseudo-gap metal acts as if it has a charge carrier

---

[1]Sachdev and Chowdhury, 2016

density equal to the doping: $n = p$. There is experimental work[2] that describes this this transition to be a very abrupt jump from $n = p$ to $n = 1 + p$ between $p = 0.16$ and $p = 0.19$. Because of this, it is often described as what is called a fractionalised Fermi liquid[3]. To build a model that predicts this fractionalised Fermi liquid, a model with dimers, rather than single electron is used. This model will be introduced in section 1.2 and the Hamiltonian that is used to get back to this phase will be introduced in section 1.3. This will be a dimer version of the Hubbard model, with a similar kinetic and potential term.

1.2 Formulation of the Dimer Model

Section 1.1.1 outlines how the usual description of electrons on a lattice is given in terms of the occupations of lattice site by said electrons. This section aims to introduce a way to describe electrons in a reduced Hilbert space. To do this, the system looks at the occupation of two neighbouring sites by two electrons as a so-called dimer, rather than per individual site. Such a dimer would have an electric charge of $2e$ (e is the electron charge) as a given. More than that, it will be defined as being Bosonic and free of spin. The creation operator of such a dimer on neighbouring sites x and y would be given by equation 1.7.

1.2.1 Introducing the Bosonic Dimer Operator

To begin, the definition of the first version of the creation operator for the Bosonic dimer is defined by equation 1.7 as a (spinless) singlet state. After section 1.2.3 an aproximation will be made, changing the properties of $D_{xy}^{(\dagger)}$ somewhat.

$$D_{xy}^{\dagger} := \frac{c_{x\uparrow}^{\dagger} c_{y\downarrow}^{\dagger} - c_{x\downarrow}^{\dagger} c_{y\uparrow}^{\dagger}}{\sqrt{2}} \tag{1.7}$$

Note that using 1.3 one finds that $D_{xy}^{\dagger} = D_{yx}^{\dagger}$, which is an important detail for the unicity of the dimer on two given sites: there is no dominant site.

Since $D_{xy}^{\dagger}$ is a superposition of two two-electron states, it is expected to be a Boson-like operator. Ideally this would follow the commutation rules for Boson. Two of these rules are trivially true, simply doubly commuting the Fermionic operators mentioned above.

$$[D_{xy}^{\dagger}, D_{x'y'}^{\dagger}] = 0 \tag{1.8}$$

$$[D_{xy}, D_{x'y'}] = 0 \tag{1.9}$$

The third commutator, on the other hand, is less straight forward than equation 1.1, as seen in equation 1.10.

$$[D_{xy}, D_{x'y'}^{\dagger}] = \delta_{xx',yy'} + \delta_{xy',yx'} + \text{rest term} \tag{1.10}$$

---

[2]Badoux, 2016, Proust and Taillefer, 2018
[3]Senthil, Sachdev, and Vojta, 2003, Punk, Allais, and Sachdev, 2015

As a first has a double Kronecker delta, and second of all, there is what will be called a "rest term", which is given in equation 1.11.

$$
\begin{aligned}
\text{rest term} = -\frac{1}{2}\Big(& \delta_{xx'}\big(c^\dagger_{y\uparrow}c_{y'\uparrow} + c^\dagger_{y\downarrow}c_{y'\downarrow}\big) + \delta_{yy'}\big(c^\dagger_{x\uparrow}c_{x'\uparrow} + c^\dagger_{x\downarrow}c_{x'\downarrow}\big) \\
& +\delta_{xy'}\big(c^\dagger_{y\uparrow}c_{x'\uparrow} + c^\dagger_{y\downarrow}c_{x'\downarrow}\big) + \delta_{yx'}\big(c^\dagger_{x\uparrow}c_{y'\uparrow} + c^\dagger_{x\downarrow}c_{y'\downarrow}\big)\Big)
\end{aligned}
\tag{1.11}
$$

Though this does not perfectly fit the Bosonic commutator, it has the same expectation value in the vacuum:

$$
\begin{aligned}
\langle 0|[D_{xy}, D^\dagger_{x'y'}]|0\rangle &= \delta_{xx',yy'} + \delta_{xy',yx'} \\
&= \delta_{\{xy\}\{x'y'\}}
\end{aligned}
\tag{1.12}
$$

The notation in equation 1.12 means that x and y must be equal to x' and y', as an unordered pair. A different and unambiguous way to name the dimers is to label each dimer by one of the sites and orientation. On the square lattice this would be of the form (i, η), where $\eta = x, y$. The two sites are then $(\vec{i}, \vec{i} + \hat{\eta})$. By not allowing η to be $-x$ or $-y$, (i, η) gives a unique way to label the dimer. On a triangular lattice the allowed values for η would be a, b and c, where $\vec{a} = (1,0)$, $\vec{b} = (-\frac{1}{2}, \frac{\sqrt{3}}{2})$ and $\vec{c} = (-\frac{1}{2}, -\frac{\sqrt{3}}{2})$, assuming the lattice constant is 1. Figure 1.2 gives a visualisation of all dimers around labelled to belong to site i. By restricting oneself to only the dimer orientations shown, double counting is avoided. The other dimers that cover site i can be made with another site: take $(i - \vec{a}, a)$ is what otherwise would have been $(i, -a)$. The choice of these dimers is made with symmetry in mind. Using this notation equation 1.12 can be rewritten to the more compact equation 1.13.

$$
\langle 0|[D_{(i,\eta)}, D^\dagger_{(i',\eta')}]|0\rangle = \delta_{ii',\eta\eta'}
\tag{1.13}
$$

This notation can be further simplified by reducing (i, η) to just i. Henceforth, dimer operators shall often be named according to equation 1.14.

$$
\begin{aligned}
i &= (i, \eta) \\
&= (i, i + \vec{\eta})
\end{aligned}
\tag{1.14}
$$

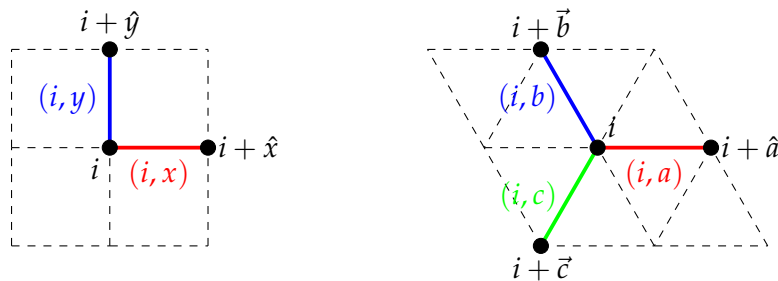In which the second line is the original two-site notation (x, y).

FIGURE 1.2: This figure shows the different dimers on site i according to the (i, η)-notation, left for the square lattice, right for the triangular lattice.

Before continuing to the next section, a short discussion of some of the limitations imposed on the notation from equation 1.7 could be useful. First of all, the definition of $D^\dagger_{xy}$ is in principle not limited to neighbouring sites. Since long distance (or non-nearest neighbour) dimers will not be discussed anywhere during this thesis, the notation will be restricted to only allow for nearest neighbours. The (i, η) notation automatically applies this restriction by only allowing certain values for η. Secondly, according to the definition in equation 1.7 it is possible to have overlapping dimers. For example, the states $\left(D^\dagger_{xy}\right)^2 |0\rangle$ and $D^\dagger_{xy} D^\dagger_{xz} |0\rangle$ both give non-zero states. Though this would describe an interesting system, this is not the type of dimer this thesis intends to discuss. Therefore the hard-core constraint is applied, not allowing overlapping dimers to exist on the same state.

1.2.2 Calculating the Overlap of Two Coverings

Now that a first definition of the dimer operator has been given in the previous section, it is time to create the basis states that will be used for the larger part of this thesis. These states will be a given lattice filled with dimers, such that there are no unoccupied sites left. Keep in mind that the the dimers are considered to be hard-core dimers, so no two dimers can have overlap on any given site. Because of this, the amount of dimers (N_{dimers}) is fixed to be half the number of lattice sites (N): $N_{dimers} = \frac{1}{2}N$. To define a covering, let $C := \{i | i = (i, \eta) \text{ s.t. } i \text{ is a dimer in the covering }\}$, and let $|C\rangle$ be the corresponding state:

$$|C\rangle = \prod_{i \in C} D^\dagger_i |0\rangle \tag{1.15}$$

The states defined in equation 1.15 will the be the states that form a basis for the dimer state space. An example of two possible dimer coverings on the square lattice is given in figure 1.3, which will be called C' and C respectively. An example of a triangular cover is shown in figure 1.4. The triangular covering has one dimer that showcases the periodic boundary conditions of the system, which is a property both the square and triangular lattice share.
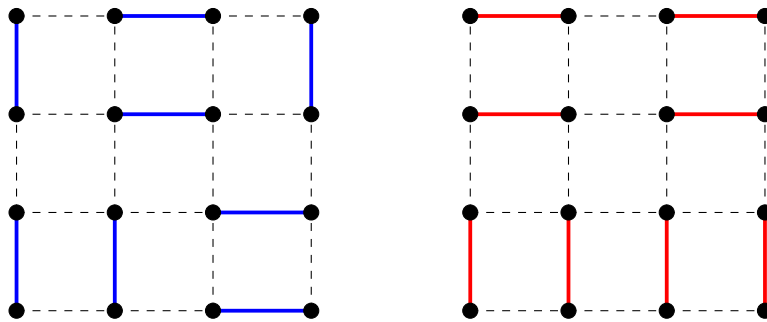
FIGURE 1.3: Examples of two dimer coverings on the square lattice. The red covering (on the right) will be named C, while the blue covering shall be called C'.

All coverings C have a corresponding state $|C\rangle$, which together form a basis for the dimer state space. Ideally this basis would be orthonormal: $\langle C'|C\rangle = \delta_{C'C}$. This would be true if the $D^\dagger_i$ operators would be perfectly (hard-core) Bosonic, but since equation 1.10 holds, this is not the case.
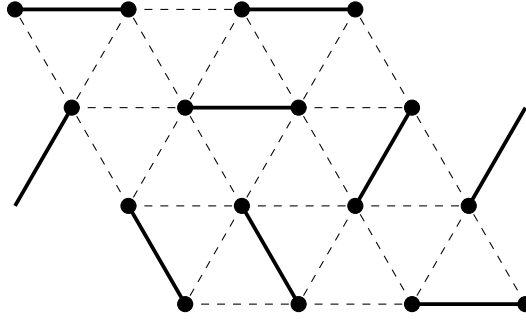
FIGURE 1.4: An example of a covering for the triangular lattice.

Using the (anti-)commutation rules for the $D_i^{(\dagger)}$ and $c_{i\sigma}^{(\dagger)}$ one can find the value of $\langle C|C \rangle$. Since there is no partial overlap between the D_i and $D_i^\dagger$ (only complete overlap), this value can be shown to be $\langle C|C \rangle = 1$. This means that the states are normalised, but not necessarily orthogonal. To calculate each individual cross section ($\langle C'|C \rangle$), one could use the same (anti-)commutation rules, but it is hard to get a general result that way.

There has been an article[4] that showed an alternative way to find the value of $\langle C'|C \rangle$. To illustrate this more graphical approach, figure 1.5 shows both square lattice coverings from figure 1.3 on the same figure. The figure has been split up into four different numbered parts, or loops. The dimers in a given loop will never have overlap with dimers from a different loop, and because of that the terms can be viewed separately. The product of these terms will be the overlap of the C' and C.
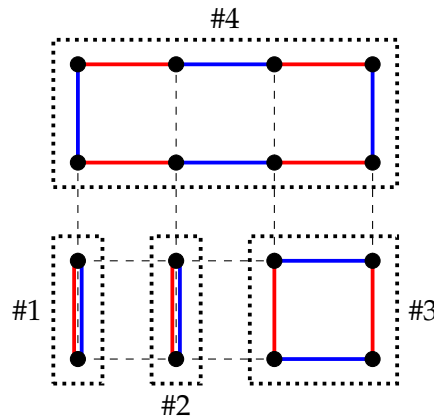
FIGURE 1.5: This figure shows the overlap of the two coverings from figure 1.3 with their respective colours kept as in the original. As is indicated by the numbers #1 to #4, this figures can be split up into four separate loops, which can be used to calculate $\langle C'|C \rangle$.

Loops #1 and #2 are barely loops, they are made because both C' and C had dimers in common, so it is clear that these terms give a 1 on as their countribution to the product. Loops #3 and #4 are more complicated, to find their contributions, one must look at what options there are to get non-zero terms. This is done by realising that a dimer is a superposition of $c_{x\uparrow}^\dagger c_{y\downarrow}^\dagger$ and $c_{x\downarrow}^\dagger c_{y\uparrow}^\dagger$, and a prefactor $\frac{1}{\sqrt{2}}$. Figure 1.6 shows part of loop #4. On the left side, the blue vertical dimer has been fixed to have ↑ (or ↓ between brackets) on the lower site and ↓ (or ↑) on the higher site. Since a non-zero term is wanted, the red dimer on the upper site is forced to fix its spin to

---

[4]Sutherland, 1988

be equal to the spin of the blue dimer: ↓ (or ↑). This fixes both sites of the red dimer as shown on the right site of figure 1.6, so now the right side of this red dimer (the upper middle site) must have spin ↑ (or ↓), which in turn fixes the blue horizontal dimer's spin on that same site. This can be extended to the entire loop, and since the loop must have en equal amount of red and blue dimers, this will always be possible.
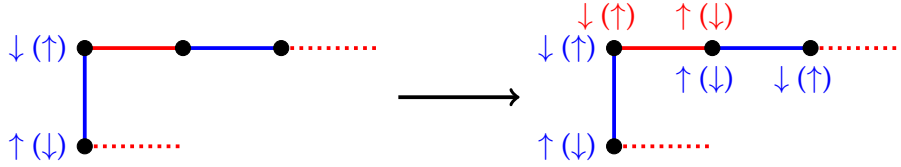

FIGURE 1.6: This figure shows what happens when choosing a spin on a given site (lowe left site) to be ↑ (or ↓). This fixes both sites of the dimer (on the left), and by extension, the entire loop (on the right).

Now, since there are two ways to fix the spins, the σ and $(-\sigma)$ choice any given site, there are two non-zero terms of the same value. This value is a result of the prefactor $\frac{1}{\sqrt{2}}$. For fixed each dimer (red and blue alike) there is one factor $\frac{1}{\sqrt{2}}$. So each loop #i contributes the factor:

$$\text{factor}_{\#i} = 2 \cdot \left(\frac{1}{\sqrt{2}} \right)^{\#\text{red dimers}+\#\text{blue dimers}}$$
$$= 2^{1-\#d_i} \tag{1.16}$$

In which #d_i is the amount of dimers (of one colour) in the loop #i. Keep in mind that equation 1.16 holds for loops such as #1 and #2 as well. Taking the product of all loop factors, $\langle C'|C \rangle$ can be found as seen in equation 1.17.

$$\langle C'|C \rangle = \prod_i 2^{1-\#d_i}$$
$$= \left(\prod_i 2 \right) \left(2^{\sum_i \#d_i} \right) \tag{1.17}$$
$$= 2^{\#\text{loops}-\#\text{dimers}}$$

As before, #dimers $= \frac{1}{2}N$, half the number of sites. For the number of loops and of dimers, the following always holds true: #dimers $\geq$ #loops. In the case that #dimers $=$ #loops, all loops consist of twice the same dimer: C and C' are identical. The smaller the number of loops (with a minimun of 1), the closer $\langle C'|C \rangle$ approaches zero.

1.2.3 Approximating Orthonormality

With this result it is possible to express how close to (or how far from) each other two states are in terms of powers of $\frac{1}{2}$ (or $\frac{1}{\sqrt{2}}$, as is often done). Identical expressed as $\left(\frac{1}{\sqrt{2}} \right)^0$, and each additional power means the two states are more different from one another. It is possible to create and expand a Hamiltonian[5] in terms of a variable

---

[5]Rokhsar and Kivelson, 1988

x, which then is the Boltzmann weight of each term. If one picks x small enough ($x = \frac{1}{\sqrt{2}}$ is small enough[6]), one can ignore terms of second order or higher. If the terms of order $\left(\frac{1}{\sqrt{2}}\right)^2$ and higher are to be ignored, then the different $|C\rangle$ would form an orthonormal basis, after all. Note that these conclusions can be drawn for not just the square lattice, but in particular for the triangular lattice too.

Hence, from this point on, the following equations are assumed true.

$$[D_i^\dagger, D_{i'}^\dagger] = 0 \tag{1.18}$$

$$[D_i, D_{i'}] = 0 \tag{1.19}$$

$$[D_i, D_{i'}^\dagger] = \delta_{ii'} \tag{1.20}$$

$$D_i|0\rangle = 0 \tag{1.21}$$

$$\langle C|C'\rangle = \delta_{CC'} \tag{1.22}$$

1.2.4 Topological Sectors and Locality

When working in the basis of coverings, the obvious way to build a Hamiltonian is in terms of covering to covering transitions. The most general Hamiltonian would then be:

$$H = \sum_{CC'} t_{CC'}|C\rangle\langle C'| + h.c. \tag{1.23}$$

In practice a Hamiltonian as the one from equation 1.23 is not needed: often it is desired to look at local interactions: local dimer displacements. Aside from nearest neighbour interactions, a good measure of how local a given interaction is, is to see how many dimers are involved. The minimal interaction would be a two-dimer interaction (for certain lattices, such the hexagonal lattice, three- or more-dimer interactions are minimal[7]). If comparing this to the orders $\left(\frac{1}{\sqrt{2}}\right)^n$ from section 1.2.3 a two-dimer interaction would have order $n = 2$. In general, an N-dimer inter action would be of order $n = 2(N-1)$, so this is consistent with the way of think from section 1.2.3.

Next it is important to define what interactions are considered local, and what interactions are not[8]. Since this thesis considers predominantly finite lattice with periodic boundary conditions, every interaction could be considered finite to a certain extent. For each interaction, a loop can be drawn. These loops have been drawn in magenta for several examples in figures 1.7 and 1.8 and consist of the dimers before and after the interaction. The distinction between local interactions and non-local is whether the given loop uses the periodicity or not. The periodic lattice is topologically equivalent to a torus, so "using the periodicity" is equivalent to having non-zero winding number on the path that the loop would take on the torus. Hence, the 2- and 4-dimer interactions in figure 1.7 are obviously local. The red interaction in figure 1.8 is local too, despite it crossing the boundary. By spatial translation, it is clear that this interaction is of the same type as the red 2-dimer interaction from figure 1.7. The blue interaction from figure 1.8 is non-local. There is no spatial translation that would make it not cross the boundaries, it is a loop around the the torus.

---

[6]Kohmoto and Shapir, 1988

[7]Moessner, Sondhi, and Chandra, 2000 briefly discusses an example, and the review article Moessner and Raman, 2008 treats many different lattices

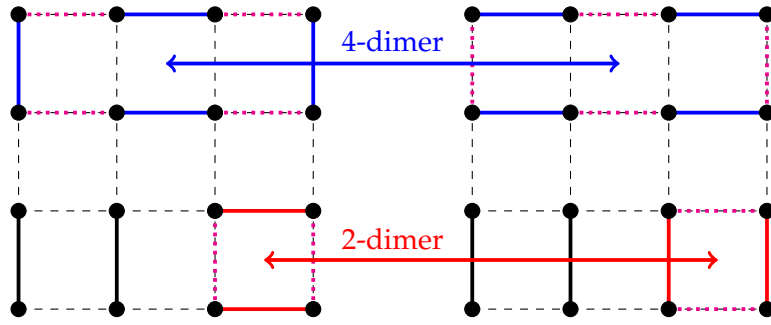[8]Sections 1.3.1 and 1.3.2 in Moessner and Raman, 2008

FIGURE 1.7: This image showcases two local interactionn: a 4-dimer interaction in blue and a 2-dimer interaction in red. The 4-dimer interaction can be recreated with three 2-dimer interactions.

A different way to determine whether an interaction is local or not, is to see if it can be reproduced by repetitions of minimal interactions. In the case of the square and triangular lattices, the minimal interactions are 2-dimer interactions on a 2×2 square of sites. These will be called "plaquette flips", from now on. For figures 1.7 and 1.8 the red interactions are already 2-dimer interactions an a 2×2 patch of sites, so they are trivially local. The blue interactions are more complex. For the 4-dimer interaction from figure 1.7, the interaction can be reproduced in three 2-dimer interactions. From the left lattice to the right: first flip the two horizontal dimers in the top-middle square, so there are four vertical dimers in a row. Then flip the top-left and top-right squares and the 4-dimer interaction has been reproduced. Note that the order of three 2-dimer interactions is $\left(\frac{1}{\sqrt{2}}\right)^{3 \cdot 2}$, which is equal to the order of one 4-dimer interaction: $\left(\frac{1}{\sqrt{2}}\right)^{2 \cdot (4-1)}$. The blue interaction from figure 1.8, even though it is strictly speaking a 2-dimer interaction, can not be reduced to plaquette flips by any means.
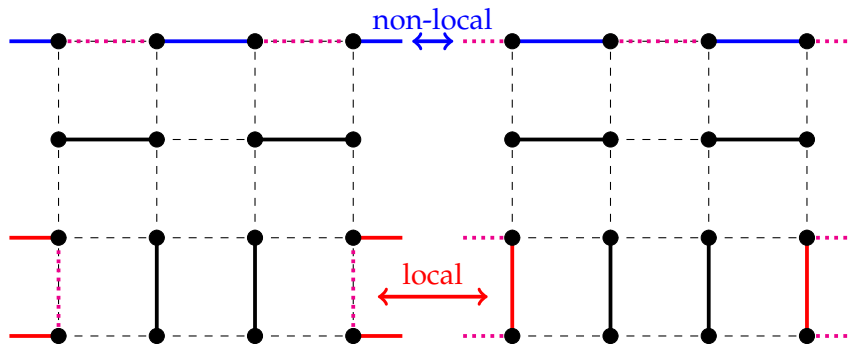
FIGURE 1.8: This image showcases two 2-dimer interactions in which the periodic boundary is crossed: a non-local interactionn in blue and a local interaction in red. The red interaction can be translated to a place on the lattice that would make it not cross the boundary, while this is not possible for the blue interaction.

The fact that certain transitions can not be reproduced by repeated local basis interactions (plaquette flips), means that if one only allows local interactions, the state space can be split up into different disconnected parts. These parts are called topological sectors and can be useful when trying to reduce the size of the state space for local calculations. All states in a given topological sector can be found by choosing two paths through the lattice (between sites). These two fixed paths

must have winding numbers (when considering the lattice as a torus, again), such that linear combinations of the two would make it possible to generate all winding numbers. In practice, this comes usually down to choosing one loop vertical and one horizontal. This path needs not necessarily be straight, as showcased in figure 1.9. To find the (topological) section number of a covering in the case of a square lattice, with given paths, one must divide all sites up into two groups. They will be called "black" and "white", since they are distributed over the sites in the same way that black and white tiles are distributed on a chess board (an example in figure 1.9). Now each dimer is covering both a black and a white lattice site. They will be given a direction (solely for determining the topological sector), namely pointing from white to black, as is indicated by the arrows in the figure. The two paths may cross some dimers, and they should be counted in two groups for each path. These two groups are the dimers that point to the left and the dimers that point to the right, with respect to the path taken. By subtracting the amount left-pointing dimers from the amount of right pointing dimers, for both paths individually, the section number is given as two integers (s_x, s_y). For figure 1.9 the section number is $(s_x, s_y) = (0, 1)$.
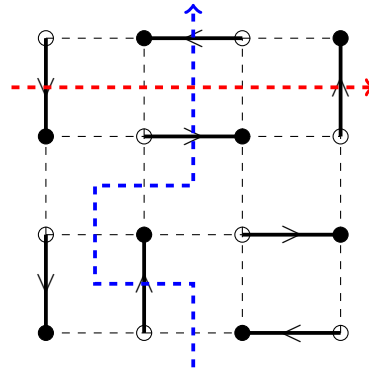

FIGURE 1.9: This figure gives an example of how to determine the topological sector of which a given covering is part. By following the red and blue arrows, on can find the *x*- and *y*-sector, respectively, by counting the amount of dimers crossed pointing to the right, minus those crossed pointing to the left (with respect to the path). The Covering in this figure is part of sector $(0, 1)$.

This section number may seem arbitrary at first, especially since there is a lot of choice in deciding how it is calculated. The paths taken are arbitrary, which tiles are white and which are black is arbitrary, the directionality of the dimers is arbitrary and the choice between (left − right) and (right − left) is arbitrary. Those last three factors only determine the sign of the winding number, so they do not matter too much (as long as chosen consistently). The reason this works, becomes clear once a fixed path is chosen. Take any covering of a certain topological section. By definition of these sections, all other coverings in this section can be creating by applying a multitude of plaquette flips. If a plaquette flip happens in a plaquette through which the path does not go, the number remains unchanged. If the path does lead through that plaquette, the path crosses two (or a multiple of two, if it crosses the plaquette more that once) potential dimers. Keep in mind: the dimers present always are opposing each other. If the path can cross through both dimers or non of the dimers, the net gain for the section number is null, so flipping between the two options does not change anything. If one dimer is crossed, the path must bend, so-to-speak, around one of the four corners/sites. Both before and after the plaquette flip, the path will cross one dimer pointing towards (or away from) that corner, so the gain

will be ± 1 in both cases. So long story short: since plaquette flips do not change the section number, and since all local interactions are repeated plaquette flips, all states in one topological sector have the same sector number for the square lattice.

For the triangular lattice the sections are somewhat different[9]: there are only two possible values per axis, so four in total. The possible values for s_x and s_z are *odd* and *even*, or 1 and 0, so it has a Z_2 topology. The reason for this is that the triangular lattice has more flippable plaquettes per lattice site: three instead of one. This allows for more possibilities in topological sector. Calculating the sector number is easier, though, is does not require considering the direction of the dimer, only the total amount of dimers crossed, modulo 2. If figure 1.9 were triangular (which would be equivalent to adding diagonal dimers, but only from lower left to upper right, in each square), its section number would be $(s_x, s_y) = (even, odd)$.

1.3 Rokhsar-Kievelson Hamiltonian

Equation 1.23 shows the most general form of a Hamiltonian working on dimer coverings. General Hamiltonians do, in principle, contain all information there possibly is to know, but unfortunately functions like this are hard to work with. Because of this, working with only local interactions (as discussed in section 1.2.4) is often a very manageable way to obtain information form otherwise complicated systems. This section takes a look at a Hamiltonian the looks at coverings in terms of their flippable plaquettes. Named after its creators, the Rokhsar-Kivelson Hamiltonian[10] for the square lattice is given as:

$$ H_{RK} = -t \sum_i \left(| \square_i \rangle \langle \,\| \,_i | + | \,\| \,_i \rangle \langle \square_i | \right) + v \sum_i \left(| \square_i \rangle \langle \square_i | + | \,\| \,_i \rangle \langle \,\| \,_i | \right) \quad (1.24) $$

The notation used is in terms of flippable plaquettes on any covering, rather than in term coverings themselves. The index i signifies which plaquette is concidered, and will from here not be written down, unless specifically needed. To remove any ambiguity on which plaquette has index i on the square lattice: the plaquette consisting of sites i, $i + \hat{x}$, $i + \hat{y}$ and $i + \hat{x} + \hat{y}$.

It is relevant to realise, is that when equation 1.24 is written in the form $H_{RK} = \sum_i H_{RK,i}$, each term $H_{RK,i}$ works on all coverings with a dimer configuration such that a flip on plaquette i is possible. To take the two example coverings from figure 1.3: the blue covering has 4 flippable plaquettes (one of them uses the periodic boundaries) and the red covering has 6 (again, one using periodic boundaries).

The Rokhsar-Kivelson (or RK-) Hamiltonian describes two interactions: a potential or static term, and a kinetic term. The potential term, whose strength is given by v can be seen as an attraction or repulsion between dimers on neighbouring sites. The kinetic term, determined by t, gives a measure of how likely it is that a given plaquette flips from horizontal to vertical (or the other way around). These two parameters v and t, together with the lattice structure itself, determine the behaviour of the system.

---

[9]Moessner and Sondhi, 2001
[10]Rokhsar and Kivelson, 1988

1.3.1   RK Hamiltonian on Triangular Lattices

The triangular version of equation 1.24 is given below, in equation 1.25. The form in this Hamiltonian is in principle identical to the square case,: it has a potential term and a kinetic term, and it can similarly be split up into parts working on a each plaquette (i, η).

$$H_{RK} = -t \sum_{i,\eta} (| \diagdown \rangle \langle \diagup | + | \diagup \rangle \langle \diagdown |) + v \sum_{i,\eta} (| \diagdown \rangle \langle \diagdown | + | \diagup \rangle \langle \diagup |) \tag{1.25}$$

The main difference for the triangular lattice compared to the square case, is that there are more plaquettes on a triangular lattice then there are on a square lattice, hence the index η. For the square lattice, one plaquette for each site suffices, but on the triangular lattice the amount of plaquettes is tripled. Similar to the naming of the dimers, the plaquatte indices (i, η) represent the site and its orientation. The allowed values for η are a, b and c, as with the dimers. Figure 1.10 visualises[11] the plaquettes alongside the dimers with the same index.
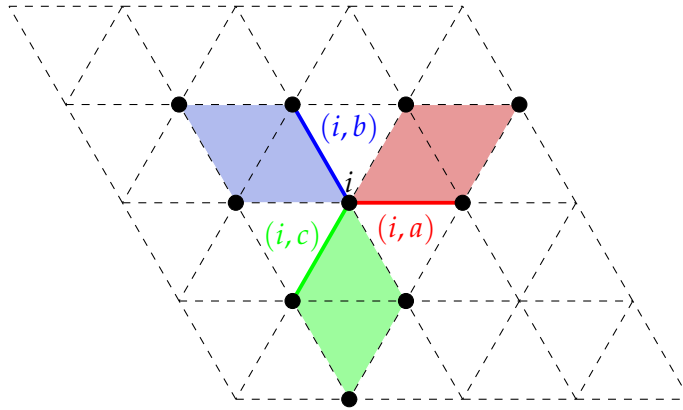
FIGURE 1.10: This figure shows all plaquettes (i, η) for a fixed i. The dimers of the same index are shown alongside them.

When working with triangular dimers in particular, it is useful to define an operation to relate the different dimer with one another. The operation η^+, and its inverse η^-, are operations to rotate orientation η to the next (or previous) orientation. For the triangular lattice, this means a rotation by $120°$ for the plus and $-120°$ for the minus. The full defining properties of these operations are given in equations 1.26 to 1.29. Since η^+ and η^- are defined symetrically and as each others inverse, the plus and minus can be swapped and the equations still hold true (with the notable exception of equation 1.28).

---

[11]For those that read this thesis without colour: (i, a) is the upper right area, (i, b) is the upper left area and (i, c) is the downward area

$$\eta = (\eta^+)^- \tag{1.26}$$

$$\eta^- = (\eta^+)^+ \tag{1.27}$$

$$a = b^-$$
$$= c^+ \tag{1.28}$$

$$\vec{\eta} = -\vec{\eta}^+ - \vec{\eta}^- \tag{1.29}$$

Using this new operation, it is possible to write down the sites of plaquette (i, η) in terms of only i and η. The sites are: i, $i + \vec{\eta}$, $i - \vec{\eta}^-$ and $i + \vec{\eta} - \vec{\eta}^-$.

There is some arbitrarity in the orientations a, b and c, though for the symmetry of this choice, and because working with $a = (-1,0)$ instead of $a = (1,0)$ feels almost dirty, the choice was very obvious. The choice of which plaquette corresponds to (i, η), however, has a lot more freedom, even whith the restriction that it must be symmetric. An alternate candidate for the sites of plaquette (i, η) would have been: i, $i + \vec{\eta}$, $i + \vec{\eta}^+$ and $i - \vec{\eta}^-$. This is slightly cleaner in notation, and compacter if drawn as in figure 1.10. The sole reason this choice was not made, is that it came to mind after most calculations requiring the (i, η) indexing had already been completed.

It is possible to create a similar operation to η^+ on the square lattice. Since there are only two relevant orientations ($\hat{x}$ and $\hat{y}$), this operation would allow for alternation between these two orientations. Geometrically this would not be a rotation, but a reflection on the line $x = y$. Then, $x^+ = y$ and $y^+ = x$, meaning that $(\eta^+)^+ = \eta$ holds on the square lattice, and making η^- redundant, since $\eta^- = \eta^+$.

1.3.2 The Staggered Phase

The RK Hamiltonian has two parameters which can be used to tune the system. The kinetic term with parameter t (often J in literature) and the static term (or potential term) with parameter v. Once a lattice has been chosen, these terms determine the behaviour of the system.

Some phases may differ for different lattices, but one that is the same for all shapes is the case where $v > |t|$ (and $v > 0$). The energy of this of any state Ψ is given by $E = \langle \Psi | H_{RK} | \Psi \rangle$. The contribution of any non-flippable plaquette is always zero (independent of v and t), so the energy would be the sum of the contributions of all flippable plaquettes. For each given plaquette, the situation can be reduced to $a| \boxed{\ } \rangle + b| \boxed{\ } \rangle$, with a and b complex numbers. There is an individual a and b for each unique pair of coverings that are equal to each other, bar plaquette i. The energy contribution of this part will be $(\bar{a}\langle \boxed{\ }| + \bar{b}\langle \boxed{\ }|) H_{RK,i} (a| \boxed{\ }\rangle + b| \boxed{\ }\rangle)$. So, this would boil down to:

$$\langle \Psi | H_{RK} | \Psi \rangle = \sum_{\text{all } (a,b)} -2t\big(\text{Re}(a)\text{Re}(b) + \text{Im}(a)\text{Im}(b)\big) + v\big(|a|^2 + |b|^2\big) \tag{1.30}$$

The triangle inequality can be applied to the right-hand side of equation 1.30 find that $\text{Im}(a)^2 + \text{Im}(b)^g eq 2\text{Im}(a)\text{Im}(b)$ and $\text{Re}(a)^2 + \text{Re}(b)^2 \geq 2\text{Re}(a)\text{Re}(b)$. This gives gives a lower limit to $\langle \Psi | H_{RK} | \Psi \rangle$, given in equation 1.31.

$$\langle \Psi | H_{RK} | \Psi \rangle \geq \sum_{\text{all } (a,b)} 2(v - t)\big(\text{Re}(a)\text{Re}(b) + \text{Im}(a)\text{Im}(b)\big) \tag{1.31}$$

Laslty, since $v > |t|$ by choice this means that $\langle \Psi | H_{RK} | \Psi \rangle > 0$ as soon as there is any covering with at least one flippable plaquette. So the ground state for $v > |t|$ are the so-called "staggered states[12]". The staggered states are all states that have no flippable plaquettes, which makes their energy nil. This conclusion holds true for all lattice-shapes, figure 1.11 shows an example of these staggered states for two different kinds of lattices: triangular and square. The staggered states are only a very small portion of the state space. On a square lattice, there are four states: the state shown in figure 1.11 can be inverted to get a second vertical staggered state, and there are the horizontal versions of these states. Since all these states are oriented in a specified direction, the staggered state breaks rotational and translational invariance. The triangular lattice does not have staggered states for all lattice sizes[13], but for lattices of $4N \times 4M$ size, there are at least twelve (the one in the figure, three spatially translated version of said lattice, and those four in two different orientations).
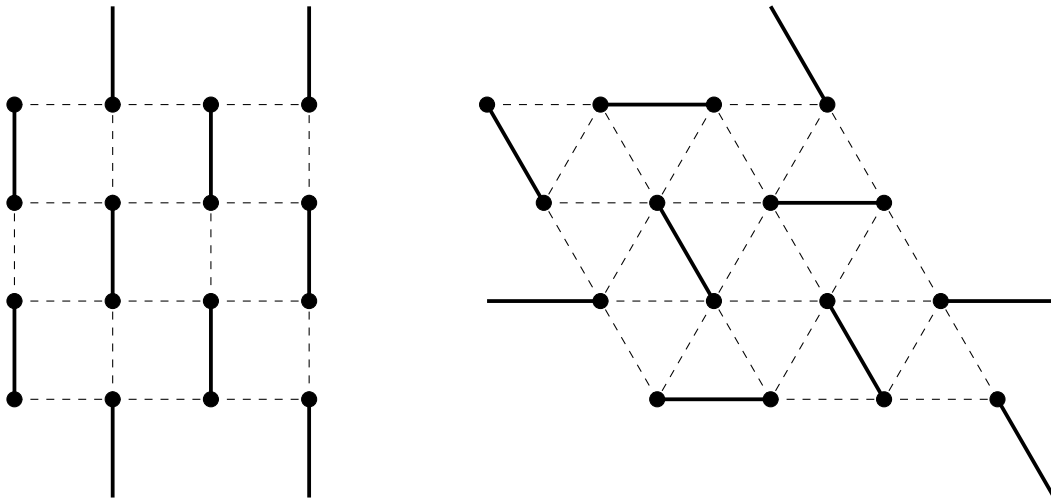
FIGURE 1.11: Examples of staggered dimer coverings on square the lattice (left) and triangular lattice (right).

1.3.3 The RK point and RVB State

The next situation to consider is the case $v = \pm t$. The same reasoning as for the staggered state can be applied for this situation, up until equation 1.30. Filling in $t = \pm v$ will give equation 1.32.

$$\langle \Psi | H_{RK} | \Psi \rangle = \sum_{\text{all } (a,b)} v \big(|a|^2 + |b|^2 \mp 2\text{Re}(a)\text{Re}(b) \mp 2\text{Im}(a)\text{Im}(b) \big) \qquad (1.32)$$

Here, the triangle inequality can be applied again, which teaches us that $\text{Im}(a)^2 + \text{Im}(b)^2 \mp 2\text{Im}(a)\text{Im}(b) \geq 0$ and $\text{Re}(a)^2 + \text{Re}(b)^2 \mp 2\text{Re}(a)\text{Re}(b) \geq 0$. It is important that this inequality can only be an equality when $\text{Im}(a) = \pm\text{Im}(b)$ and $\text{Re}(a) = \pm\text{Re}(b)$. Or with other words, all for all a and b: $a = \pm b$. This would mean that $\langle \Psi | H_{RK} | \Psi \rangle = 0$ if $|\psi_{RK}\rangle$ is a superposition of all coverings with flippable plaquettes (all non-staggered coverings). For $v = t$ all coefficients would be equal and for $v = -t$ all coefficients amplitudes would be equal amplitude, but with alternating

---

[12]Moessner and Raman, 2008
[13]See figure 4.4 in section 4.1.3

sign. This sign of a covering $|C\rangle$ would then be $(-1)^n$, where n is the amount of plaquette flips needed to reach C in its topological sector from an arbitrary begin state (within that sector).

If t is assumed to be positive, the only parameter to be considered in a phase diagram is the ratio of t and v. The point where this ratio is 1 is called the Rokhsar-Kievelson point (sometimes line), after the people that originally found this ground state. This state is unique because it is what is called a resonating valence bond state[14] or RVB liquid. These states, in general, are not necessarily equal weight, there can be some deviations, as long as the system is singlet (no spin), the gauge symmetry (Z_2 for triangular H_{RK}, $U(1)$ for square) is not broken and the system keeps its translational and rotational invariance.

It is important that the ground state on the RK point is degenerate. Both the RVB state (or alternating RVB state) and the staggered states have zero energy. So the ground state is a superposition of staggered states and RVB states, allowing for degeneracy in the ground state. Further degeneracy in the ground state comes from the fact that there is a separate RVB state for each topological sector. To reduce the degeneracy, the RVB-state are defined per sector, since numerics and analytics can be limited to one sector.

The RVB phase is something that is not necessary restricted to the RK point. Depending on the lattice, this phase can extend into the regions where $|t| > v$ (and $t \geq 0$). The square lattice has the RVB state is a $U(1)$ spin liquid[15]. Because of this, its symmetry breaks away from the RK point, so the RVB phases is limited to this point. On systems with a Z_2 gauge symmetry, like the RK-Hamiltoniian on the triangular lattice, the RK point goes from a unique critical point to an actual new phase (see figure 1.13). The symmetry is not broken as easy as in the case of a square lattice H_{RL} ($U(1)$ symmetry). The RVB state away from the RK point is slightly different from the state exactly on said point, in the sense that it is not an equal weight superposition of all states anymore. In particular (but not limited to only this), there are no more staggered states in the RVB spin liquid outside the RK point.

1.3.4 The Columnar Phase

Now consider the regime where $v < -|t| \leq 0$. Since v is negative, and larger than $|t|$ in absolute value, each flippable plaquette on a covering lowers the energy of the state. The ground states are the coverings with the most possible flippable plaquettes. This is a state with only dimers in the smae direction, parallel to each other. Examples of these states are given in figure 1.12. Keep in mind that even though the shown triangular columnar state looks similar to the staggered square state from figure 1.12, it certainly is columnar: triangular lattices have more flippable plaquettes than square lattices. These states have an energy of $E = \frac{N}{2}v$. It is possible to create states that get a negative contribution from the kinetic part of the RK Hamiltonian. But by doing so, the coefficient of the fully columnar states becomes smaller, so the total energy would be higher than that of the columnar state. For the square lattice, there is a degeneracy of 4 in the ground state, for the triangular lattice this is larger, and even proportional to the lattice size. This state too breaks rotational symmetry.

---

[14]Moessner and Sondhi, 2001 and Anderson, 1987
[15]Fradkin and Kivelson, 1990
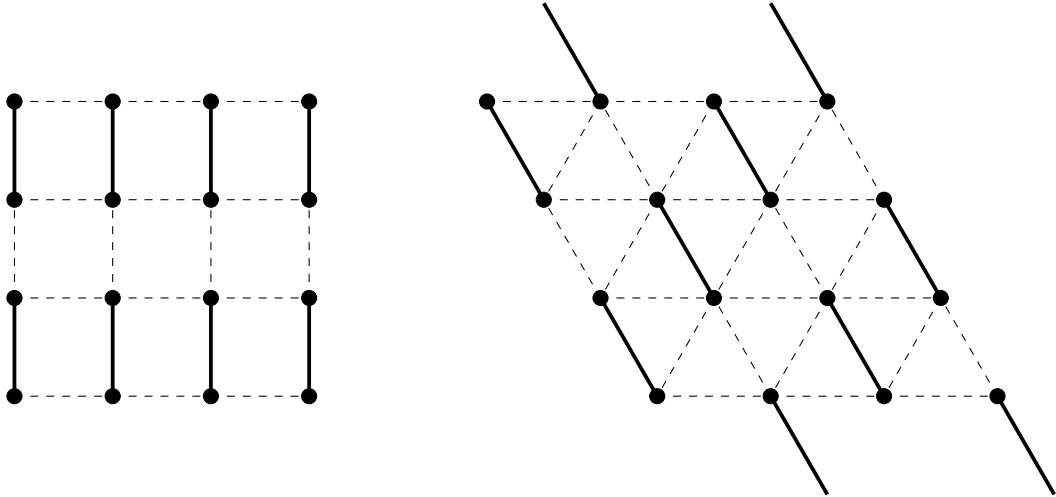
FIGURE 1.12: Examples of columnar dimer coverings on the square
lattice (left) and triangular lattice (right).

1.3.5   Completing the Phase Diagram

With all the different found ground states for different regimes in section 1.3.2 to
1.3.4 it is possible to create part of a phase diagram. This is done in figure 1.13,
though there are a few caveats. Where the RVB state begins and ends is not clear for
all lattices, and for for some lattices it does not reach beyond the RK line. Numerical
simulations [16] indicate that the RVB phase of the triangular lattice lies between $0.8 <
\frac{v}{t} < 1.0$. In addition to this, the part of the RVB phase for $t < 0$ is the alternating
variant[17].
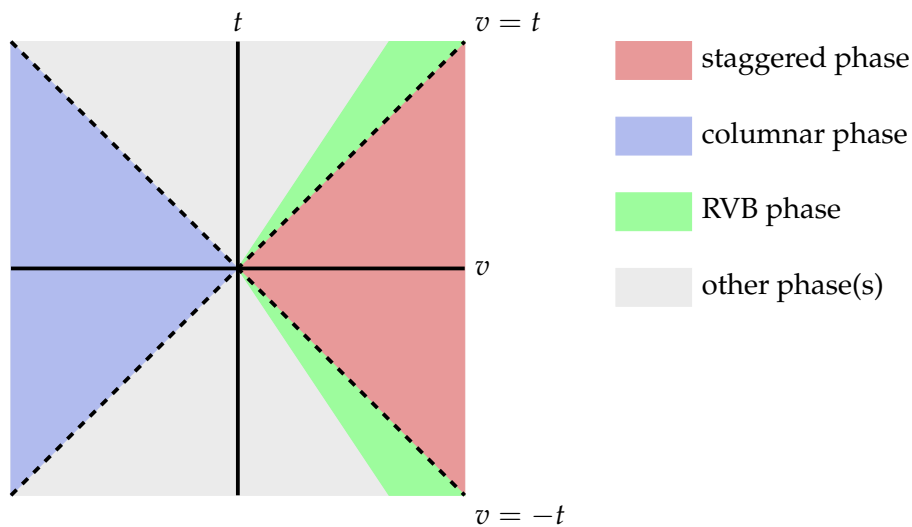
FIGURE 1.13: This figure shows the phase diagram for the RK model.
Keep in mind that the RVB phase only extends beyond the RK line
($v = \pm t$) if the system has a Z_2 symmetry, like the triangular H_{RK}.
The other phase is for a large part unknown, with the exception of
some very specific cases.

---

[16]Ralko et al., 2005
[17]Some research has been done to states similar to the alternating RVB state, where this state is
called a "vison", see Senthil and Fisher, 2000 for more on this

The other phase(s)
footnoteMoessner and Raman, 2008 in figure 1.13 are generally not known, though parts of it are known. For the triangular lattice there is a certain phase called the $\sqrt{12} \times \sqrt{12}$ phase, since it has a 12-site unit cell. For several bipartite lattices, such as the square lattice and honeycomb, there exists another phase called the plaquette state (partially in the same regime as the RVB phase for other lattices) and there are certain ideas based around ver large unit cells of 36 sites and similar [18]. Most of these more exotic phases will not be relevant for this thesis.

[18] read Zeng and Elser, 1995 for 36 sites at once and Nikolic and Senthil, 2003 for more on the kagomé lattice

Chapter 2

Classical Dimer Correlations on the Triangular Lattice

This chapter will be dedicated to the calculation of the classical correlation functions for dimers on a triangular lattice. This is done, because they are needed in chapter 3 to be able to complete the calculation of the ground state, there. The methods used are similar in approach to the calculation of the classical dimer correlations in Johannes Feldmeier's work[1].

This chapter was originally supposed to be merely a section in chapter 3, but due to the difference in complexity of the square and triangular lattice, this grew out to become its own chapter.

2.1 Setting Up the Grassman Variables

One way to calculate the classical correlation function for two variables of any kind, is to set up a field theory. Since the dimers described in chapter 1 are Bosonic, one's first intuition would likely be to create Bosonic variables corresponding to each dimer. But since dimers are described to be on two separated sites, it makes more sense to describe the dimers as a combination of two Fermionic variables on separate sites. This naturally includes the hard-core constraint of the dimers, since the variables used will be Grassman variables.

Grassman variable or Grassman numbers are number-like variables named after (surprise, surprise!) Hermann Grassman. The main property of Grassman numbers is that they anticommute, and because of this, the square of a Grassman variable is naught. To create a field theory, one needs to find an appropriate action $S[\eta, \bar{\eta}]$, where η and $\bar{\eta}$ are the Grassman numbers used to describe the dimers. Then, using this action it is possible to find the partition function and calculate the correlation functions.

$$Z = \int D[\eta, \bar{\eta}]e^{S[\eta, \bar{\eta}]} \tag{2.1}$$

$$\langle \eta_i \bar{\eta}_j \rangle = \frac{1}{Z} \int D[\eta, \bar{\eta}] \eta_i \bar{\eta}_j e^{S[\eta, \bar{\eta}]} \tag{2.2}$$

So the first thing to do, is to create an action that describes all possible dimers on a lattice. To do so, it is useful to take a look at a unit cell of the triangular lattice, which for this purpose is 2×2 lattice sites, as shown in figure 2.1. This unit cell can be repeated to fill the entire lattice with dimers. To use the dimers, they need to be given a directinality such that hat every circular path of even length on the lattice

---

[1]section 2.2 of Feldmeier, 2018

(from site to site to site) is clockwise odd[2]. This means that if one follows this path (of even length) in clockwise direction, the amount of counterclockwise pointing dimers is odd. The lattice in figure 2.1 is clockwise odd[3], though this is not a unique choice. This thesis will stick with the convention given in the figure.
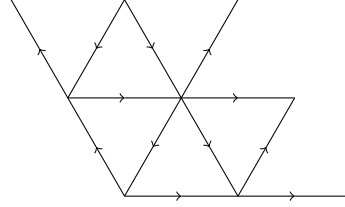
FIGURE 2.1: This figure shows a unit cell of the triangular lattice in terms of all possible dimers, drawn with their directionalities given by the arrows.

In addition to this, it is necessary to split the lattice up into two types of sites, denoted by $\circ$ and $\times$. In addition to that, each unit cell gets assigned an index (m, n), such that the sites in each unit cell are called $\big(2m(+1), 2n(+1)\big)$, figure 2.2 shows this.
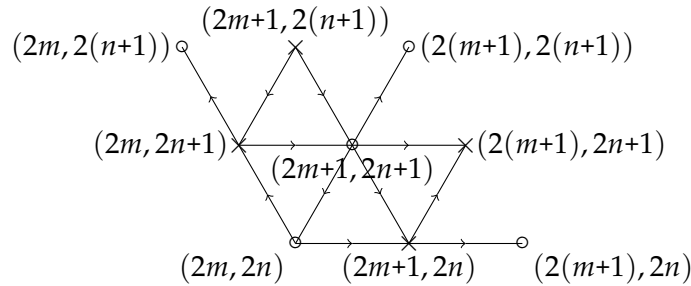
FIGURE 2.2: This figure shows the same unit cell as figure 2.1, but with the labeling of the sites added.

Now that an example unit cell has been created, is is time to associate variables with lattice sites. The sites will be split up into two sets of Grassman numbers, the η_i correspond to the $\circ$-sites and the $\bar{\eta}_i$ correspond to the $\times$-sites. Now, if a dimer points from site i to site j, the variable with index i will be written first. Since the variable are anticommuting, this is a way to assign sign to the dimers. All possible dimers for sites i and j are shown in figure 2.3. It is important to realise that there is no relation between variable η_i and $\bar{\eta}_i$, other than that they both happen to be assigned to the same site. For normal (commuting) variables, the bar would indicate a complex conjugate. The bar is only present on Grassman variables to be consistent with the notation of commuting fields, but has not inherent meaning.

The action $S[\eta, \bar{\eta}]$ can now be written as a sum of all dimers on each unit cell. But to restrict the partition function to only close packed coverings, an opposite close packed reference covering is needed. It is opposite in the sense that its arrows point in the opposite direction and its $\circ$- and $\times$-sites have been swapped. This additional term ensures that only well-defined coverings are allowed. The reference covering used in this thesis is shown in figure 2.4.

---

[2]Kasteleyn, 1961 gives a very mathematically rigourous and precise set of conditions for which this method can be applied

[3]This example was found by Fendley, Moessner, and Sondhi, 2002

i	j	notation
✕———→———o		$\bar{\eta}_i \eta_j$
o———←———✕		$\bar{\eta}_j \eta_i$
✕———←———o		$\eta_j \bar{\eta}_i$
o———→———✕		$\eta_i \bar{\eta}_j$
o———→———o		$\eta_i \eta_j$
o———←———o		$\eta_j \eta_i$
✕———→———✕		$\bar{\eta}_i \bar{\eta}_j$
✕———←———✕		$\bar{\eta}_j \bar{\eta}_i$

FIGURE 2.3: This figure shows all possible ways a dimer could be written down on two sites i and j with the corresponding notation in Grassman numbers.
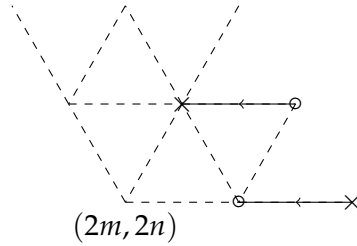
$(2m, 2n)$

FIGURE 2.4: This figure shows the example reference filling used during the calculation, with site $(2m, 2n)$ as a reference point.

Together, the reference coverings and all allowed dimer form the action of the classical triangular dimer model: $S[\eta, \bar{\eta}] = \sum_{m,n} \text{dimers} + \sum_{m,n} \text{reference}$. The full corresponding equation can be seen in equation 2.3. The first twelve terms (or first four lines) are the possible dimers in the unit cell, and the final two terms are the reference covering.

$$
\begin{aligned}
S[\eta, \bar{\eta}] = \sum_{m,n} \Big(\ & \eta_{2m,2n}\bar{\eta}_{2m+1,2n} + \bar{\eta}_{2m+1,2n}\eta_{2m+2,2n} + \eta_{2m,2n}\bar{\eta}_{2m,2n+1} \\
& + \eta_{2m+1,2n+1}\eta_{2m,2n} + \eta_{2m+1,2n+1}\bar{\eta}_{2m+1,2n} + \bar{\eta}_{2m+1,2n}\bar{\eta}_{2(m+1),2n+1} \\
& + \bar{\eta}_{2m,2n+1}\eta_{2m+1,2n+1} + \eta_{2m+1,2n+1}\bar{\eta}_{2(m+1),2n+1} + \bar{\eta}_{2m,2n+1}\eta_{2m,2(n+1)} \\
& + \bar{\eta}_{2m+1,2(n+1)}\bar{\eta}_{2m,2n+1} + \bar{\eta}_{2m+1,2(n+1)}\eta_{2m+1,2n+1} + \eta_{2m+1,2n+1}\eta_{2(m+1),2(n+1)} \\
& + \bar{\eta}_{2(m+1),2n}\eta_{2m+1,2n} + \eta_{2(m+1),2n+1}\bar{\eta}_{2m+1,2n+1} \Big)
\end{aligned}
$$

$$(2.3)$$

Since the action has such an inconveniently large summand, it is often useful to write the action down as $S[\eta, \bar{\eta}] = \sum_{m,n} S_{mn}$. These terms S_{mn} will be further looked into during the next section, in order to find expressions for Z and $\langle \eta_i \bar{\eta}_j \rangle$ that can be used for numerical (and in some few cases even exact) analysis.

2.2   Computation of the Two-Variable Correlation

In principle, it is possible of any finite-sized lattice to write the action from equation 2.3 in the form $S[\eta, \bar{\eta}] = \sum_{\alpha, \beta} \eta_\alpha M_{\alpha\beta} \eta_\beta$. The indices α and β would include both the site and whether there is a bar on the η or not. The problem with this, is that there is no simple-to-work-with form in which to write the matrix M. So a work-around is needed, for which the following transformations will be used:

$$\eta_{2m,2n} = \int \frac{dpdq}{(2\pi)^2} e^{i\vec{p}\cdot\vec{m}} \chi_{\vec{p}}^1$$

$$\eta_{2m+1,2n} = \int \frac{dpdq}{(2\pi)^2} e^{i\vec{p}\cdot\vec{m}} \chi_{\vec{p}}^2$$

$$\eta_{2m,2n+1} = \int \frac{dpdq}{(2\pi)^2} e^{i\vec{p}\cdot\vec{m}} \chi_{\vec{p}}^3$$

$$\eta_{2m+1,2n+1} = \int \frac{dpdq}{(2\pi)^2} e^{i\vec{p}\cdot\vec{m}} \chi_{\vec{p}}^4$$

$$\bar{\eta}_{2m,2n} = \int \frac{dpdq}{(2\pi)^2} e^{i\vec{p}\cdot\vec{m}} \bar{\chi}_{\vec{p}}^1 \qquad (2.4)$$

$$\bar{\eta}_{2m+1,2n} = \int \frac{dpdq}{(2\pi)^2} e^{i\vec{p}\cdot\vec{m}} \bar{\chi}_{\vec{p}}^2$$

$$\bar{\eta}_{2m,2n+1} = \int \frac{dpdq}{(2\pi)^2} e^{i\vec{p}\cdot\vec{m}} \bar{\chi}_{\vec{p}}^3$$

$$\bar{\eta}_{2m+1,2n+1} = \int \frac{dpdq}{(2\pi)^2} e^{i\vec{p}\cdot\vec{m}} \bar{\chi}_{\vec{p}}^4$$

The transformation in equation 2.4 is the same for all η and $\bar{\eta}$ alike, in particular: the sign of the exponent is the same independent of the bar. The vectors $\vec{p} = (p, q)$ and $\vec{m} = (m, n)$ are the normal and reciprocal lattice vectors of the lattice of the unit cells. This means that these lattice vectors are double the length of the vectors of the original triangular lattice.

$$\int \frac{dpdq}{(2\pi)^2} := \frac{1}{N} \sum_{\vec{p}} \qquad (2.5)$$

The integral in equation 2.4 is abuse of notation. As long as there is a Grassman number in the integral it will always be a sum over all reciprocal lattice vectors $\vec{p}$, as shown in equation 2.5. Once the Grassman variables have been removed, it is possible to take the limit to an actual integral, if the lattice is assumed to be large: $N \to \infty$, with N the number of vectors over which the sum runs (this is not the number of lattice sites).

$$\sum_{\vec{m}} \eta_{\vec{m}+\vec{a}}^\alpha \eta_{\vec{m}+\vec{b}}^\beta = \frac{1}{N^2} \sum_{\vec{m}\vec{p}\vec{p}'} e^{i\vec{m}\cdot(\vec{p}+\vec{p}')+i(\vec{a}\cdot\vec{p}+\vec{b}\cdot\vec{p}')} \chi_{\vec{p}}^\alpha \chi_{\vec{p}'}^\beta$$

$$= \frac{1}{N^2} \sum_{\vec{p}\vec{p}'} \left(\sum_{\vec{m}} e^{i\vec{m}\cdot(\vec{p}+\vec{p}')} \right) e^{i(\vec{a}\cdot\vec{p}+\vec{b}\cdot\vec{p}')} \chi_{\vec{p}}^\alpha \chi_{\vec{p}'}^\beta \qquad (2.6)$$

Using equations 2.4 and 2.5 the action can be rewritten as a sum over $\vec{m}$, $\vec{p}$ and $\vec{p}'$, where the summand is the transformed version of the 14 dimers from equation 2.3.

Each of these 14 terms can be written down in the same form shown in equation 2.6. The part between brackets can be rewritten according to equation 2.7.

$$\sum_{\vec{m}} e^{i\vec{m}\cdot(\vec{p}+\vec{p}')} = N\delta_{\vec{0},\vec{p}+\vec{p}'}$$ (2.7)

Combining if then the sum over $\vec{p}'$ is taken, this Kronecker delta gives $\vec{p} + \vec{p}' = 0$ which is then used to eliminate p', resulting in equation 2.8.

$$\begin{aligned}
\sum_{\vec{m}} \eta^{\alpha}_{\vec{m}+\vec{a}}\eta^{\beta}_{\vec{m}+\vec{b}} &= \frac{1}{N}\sum_{\vec{p}\vec{p}'}\delta_{\vec{0},\vec{p}+\vec{p}'}e^{i(\vec{a}\cdot\vec{p}+\vec{b}\cdot\vec{p}')}\chi^{\alpha}_{\vec{p}}\chi^{\beta}_{\vec{p}'} \\
&= \frac{1}{N}\sum_{\vec{p}}e^{i(\vec{a}-\vec{b})\cdot\vec{p}}\chi^{\alpha}_{\vec{p}}\chi^{\beta}_{-\vec{p}} \\
&= \int \frac{d^2p}{(2\pi)^2}e^{i(\vec{a}-\vec{b})\cdot\vec{p}}\chi^{\alpha}_{\vec{p}}\chi^{\beta}_{-\vec{p}}
\end{aligned}$$ (2.8)

By anticommuting $\eta^{\alpha}_{\vec{m}+\vec{a}}$ and $\eta^{\beta}_{\vec{m}+\vec{b}}$ before anything else and then repeating all steps from equation 2.6 to 2.8, equation 2.9 can be obtained as well.

$$\sum_{\vec{m}} \eta^{\alpha}_{\vec{m}+\vec{a}}\eta^{\beta}_{\vec{m}+\vec{b}} = -\int \frac{d^2p}{(2\pi)^2}e^{-i(\vec{a}-\vec{b})\cdot\vec{p}}\chi^{\beta}_{\vec{p}}\chi^{\alpha}_{-\vec{p}}$$ (2.9)

This result can be applied on each of the 14 terms of the action, to eventually obtain a matrix form for the action in equation 2.10.

$$S[\eta,\bar{\eta}] = \int \frac{d^2p}{(2\pi)^2}\vec{\chi}^{T}_{\vec{p}}M'(\vec{p})\vec{\chi}_{-\vec{p}}$$ (2.10)

Where $M'(\vec{p})$ is given by equation 2.11 and $\vec{\chi}^{T}_{\vec{p}} = (\chi^{1}_{\vec{p}}, \chi^{2}_{\vec{p}}, \chi^{3}_{\vec{p}}, \chi^{4}_{\vec{p}}, \bar{\chi}^{1}_{\vec{p}}, \bar{\chi}^{2}_{\vec{p}}, \bar{\chi}^{3}_{\vec{p}}, \bar{\chi}^{4}_{\vec{p}})$.

$$M'(\vec{p}) = \begin{pmatrix}
0 & 0 & 0 & 0 & 0 & 1 & 1 & 0 \\
0 & 0 & 0 & 0 & 0 & 0 & 0 & 0 \\
0 & 0 & 0 & 0 & 0 & 0 & 0 & e^{ip(1,0)} \\
1+e^{-ip(1,1)} & 0 & 0 & 0 & 0 & 1 & e^{-ip(1,0)} & 0 \\
0 & e^{ip(1,0)} & 0 & 0 & 0 & 0 & 0 & 0 \\
e^{-ip(1,0)} & 0 & 0 & e^{ip(0,1)} & 0 & 0 & e^{-ip(1,0)}+e^{ip(0,1)} & 0 \\
e^{-ip(0,1)} & 0 & 0 & 1 & 0 & 0 & 0 & 0 \\
0 & 0 & 0 & 0 & 0 & 0 & 0 & 0
\end{pmatrix}$$ (2.11)

In which $p(x,y) = \vec{p}\cdot(\vec{a}-\vec{b})$ for all $\eta^{\alpha}\eta\beta$-terms. The matrix-term $\vec{\chi}^{T}_{\vec{p}}M'(\vec{p})\vec{\chi}_{-\vec{p}}$ can be rewritten using the equation 2.9. This would be the same as preforming three actions on the current matrix: transposing, multiplying by -1 and lastly substituting $\vec{p}$ by $-\vec{p}$. So $\vec{\chi}^{T}_{\vec{p}}M(\vec{p})\vec{\chi}_{-\vec{p}} = \vec{\chi}^{T}_{\vec{p}}\big(-M'^{T}(-\vec{p})\big)\vec{\chi}_{-\vec{p}}$. To make the matrix more symmetric, the choice made will be to write $\frac{1}{2}\vec{\chi}^{T}_{\vec{p}}M(\vec{p})\vec{\chi}_{-\vec{p}}$, where $M(\vec{p})$ is defined as in equation 2.12.

$$\frac{1}{2}M(\vec{p}) = \frac{1}{2}\left(M'(\vec{p}) - M'^{T}(-\vec{p})\right) \tag{2.12}$$

The resulting matrix will $M(\vec{p})$ then be:

$$
\begin{pmatrix}
0 & 0 & 0 & -1-e^{ip(1,0)} & 0 & 1-e^{ip(1,0)} & 1-e^{ip(0,1)} & 0 \\
0 & 0 & 0 & 0 & -e^{-ip(1,0)} & 0 & 0 & 0 \\
0 & 0 & 0 & 0 & 0 & 0 & 0 & e^{ip(1,0)} \\
1+e^{-ip(1,1)} & 0 & 0 & 0 & 0 & 1-e^{-ip(0,1)} & e^{-ip(1,0)}-1 & 0 \\
0 & e^{ip(1,0)} & 0 & 0 & 0 & 0 & 0 & 0 \\
e^{-ip(1,0)}-1 & 0 & 0 & e^{ip(0,1)}-1 & 0 & 0 & e^{-ip(1,0)}+e^{ip(0,1)} & 0 \\
e^{-ip(0,1)}-1 & 0 & 0 & 1-e^{ip(1,0)} & 0 & -e^{ip(1,0)}-e^{-ip(0,1)} & 0 & 0 \\
0 & 0 & -e^{-ip(1,0)} & 0 & 0 & 0 & 0 & 0
\end{pmatrix}
$$

$$\tag{2.13}$$

The with the matrix $M(\vec{p})$, it is now possible to rewrite the action to equation 2.14.

$$S[\eta,\bar{\eta}] = \frac{1}{2}\int \frac{d^2 p}{(2\pi)^2}\vec{\chi}_{\vec{p}}^{T}M(\vec{p})\vec{\chi}_{-\vec{p}} \tag{2.14}$$

The matrices $M(\vec{p})$ have the shape 8×8, but the action can be seen as one very large $8N \times 8N$ matrix if one combines the sum over $\vec{p}$ with $M(\vec{p})$. This large matrix $M_{8N \times 8N}$ would have the N 8×8-matrices as its diagonal terms, as shown in equation 2.15.

$$M_{8N \times 8N} = \begin{pmatrix} M(1) & 0 & \dots & 0 \\ 0 & M(2) & & \vdots \\ \vdots & & \ddots & 0 \\ 0 & \dots & 0 & M(N) \end{pmatrix} \tag{2.15}$$

The argument of the $M(i)$ is then the ith unit cell of the reciprocal lattice. Keep in mind that the values for p are cyclic, thus the final vector becomes $\vec{\chi}^{T} = (\vec{\chi}_1^{T}, \vec{\chi}_2^{T}, \dots, \vec{\chi}_N^{T})$. This same cyclicity, in combination with equations 2.8 and 2.9 ensures that $M_{8N \times 8N}$ is anti-symmetric. Now, it is possible to fill in equation 2.1: $Z = \int D[\eta]e^{S[\eta]} = \int D[\eta]\exp\left(\frac{1}{2}\vec{\chi}^{T}M_{8N \times 8N}\vec{\chi}\right)$ Use from now on the short-hand notation: $S[\eta] = S[\eta,\bar{\eta}]$. Next, rewrite the transformation in equation 2.4 as:

$$\begin{aligned} \vec{\eta} &= A\vec{\chi} \\ \vec{\chi} &= A^{-1}\vec{\eta} \end{aligned} \tag{2.16}$$

This gives the following value for the partition function:

$$Z = \int D[\eta]e^{\frac{1}{2}(A^{-1}\vec{\eta})^{T}M_{8N \times 8N}(A^{-1}\vec{\eta})} \tag{2.17}$$

Equation 2.18 offers a way[4] to rewrite equation 2.17 as an integral over χ.

$$\int D[\psi]f(\psi) = \det T \int D[\xi]f(T^{-1}\vec{\xi}) \tag{2.18}$$

In equation 2.18 $\vec{\xi} = T\vec{\psi}$. For η and χ, $\vec{\chi} = A^{-1}\eta$, and $\det A^{-1} = \frac{1}{\det A}$, so this turns equation 2.17 into equation 2.19 and eventually equation 2.20.

$$
\begin{aligned}
Z &= \frac{1}{\det A} \int D[\chi] \exp\left(\frac{1}{2}\left((A^{-1})^{-1}\vec{\chi}\right)^T M_{8N\times 8N}(A^{-1})^{-1}\vec{\chi}\right) \\
&= \frac{1}{\det A} \int D[\chi] \exp\left(\frac{1}{2}\vec{\chi}^T M_{8N\times 8N}\vec{\eta}\right)) \tag{2.19}
\end{aligned}
$$

$$= \frac{\sqrt{\det M_{8N\times 8N}}}{\det A} \tag{2.20}$$

The last thing to calculate is the actual correlation function $\langle \eta_i^\alpha \eta_j^\beta \rangle$, as given in equation 2.2. Up until equation 2.19, the same steps can be taken for the correlation function. Since $(A^{-1})^{-1}\vec{\chi} = \vec{\eta}$, filling in $(A^{-1})^{-1}\vec{\chi}$ in both η_i^α and η_j^β gives $\int \frac{d^2p}{(2\pi)^2}e^{i\vec{p}\cdot\vec{i}}\chi_{\vec{p}}^\alpha$ and $\int \frac{d^2p'}{(2\pi)^2}e^{i\vec{p}'\cdot\vec{j}}\chi_{\vec{p}'}^\beta$, respectively. These terms can thus be found in equation 2.21.

$$\langle \eta_i^\alpha \eta_j^\beta \rangle = \frac{1}{Z}\frac{1}{\det A} \int D[\chi] \left(\int \frac{d^2p}{(2\pi)^2}e^{i\vec{p}\cdot\vec{i}}\chi_{\vec{p}}^\alpha\right)\left(\int \frac{d^2p'}{(2\pi)^2}e^{i\vec{p}'\cdot\vec{j}}\chi_{\vec{p}'}^\beta\right)e^{\frac{1}{2}\vec{\chi}^T M_{8N\times 8N}\vec{\chi}} \tag{2.21}$$

Since $\int \frac{d^2p}{(2\pi)}$ is only a sum, and $\frac{1}{Z} = \frac{\det A}{\sqrt{\det M_{8N\times 8N}}}$, equation 2.21 can be reordered to:

$$
\begin{aligned}
\langle \eta_i^\alpha \eta_j^\beta \rangle &= \frac{1}{\sqrt{\det M_{8N\times 8N}}} \int \frac{d^2p\,d^2p'}{(2\pi)^4}e^{i(\vec{p}\cdot\vec{i}+\vec{p}'\cdot\vec{j})} \int D[\chi]\chi_{\vec{p}}^\alpha\chi_{\vec{p}'}^\beta e^{\frac{1}{2}\vec{\chi}^T M_{8N\times 8N}\vec{\chi}} \\
&= -\int \frac{d^2p\,d^2p'}{(2\pi)^4}e^{i(\vec{p}\cdot\vec{i}+\vec{p}'\cdot\vec{j})}\left(M_{8N\times 8N}^{-1}\right)_{\vec{p}\vec{p}',\alpha\beta} \tag{2.22}
\end{aligned}
$$

The inverse matrix $M_{8N\times 8N}^{-1}$ can be found using equation 2.23, where $M(i) = M_i$ and I_8 is the 8×8 identity matrix.

$$
\begin{pmatrix} M_1 & 0 & \dots & 0 \\ 0 & M_1 & & \vdots \\ \vdots & & \ddots & 0 \\ 0 & \dots & 0 & M_N \end{pmatrix}
\begin{pmatrix} M_1^{-1} & 0 & \dots & 0 \\ 0 & M_2^{-1} & & \vdots \\ \vdots & & \ddots & 0 \\ 0 & & \dots & 0 & M_N^{-1} \end{pmatrix}
=
\begin{pmatrix} I_8 & 0 & \dots & 0 \\ 0 & I_8 & & \vdots \\ \vdots & & \ddots & 0 \\ 0 & \dots & 0 & I_8 \end{pmatrix} \tag{2.23}
$$

So the inverse of $M_{8N\times 8N}^{-1}$ is the diagonal matrix with all inverses $M^{-1}(i)$ on the diagonal. Because of this, $(M_{8N\times 8N}^{-1})_{\vec{p}\vec{p}',\alpha\beta}$ is only non-zero if $\vec{p} = -\vec{p}'$. So $(M_{8N\times 8N}^{-1})_{\vec{p}\vec{p}',\alpha\beta} = N\delta\vec{p}, -\vec{p}'M^{-1}(\vec{p})_{\alpha\beta}$. Because of this, the final form of $\langle \eta_i^\alpha \eta_j^\beta \rangle$ is given by:

---

[4]equation 2.5 from Samuel, S., 1980

$$\langle \eta_{\vec{i}}^{\alpha} \eta_{\vec{j}}^{\beta} \rangle = - \int \frac{d^2 p}{(2\pi)^2} e^{i\vec{p}\cdot(\vec{i}-\vec{j})} M^{-1}(\vec{p})_{\alpha\beta} \tag{2.24}$$

The matrix $M^{-1}(\vec{p})$ is painfully large: it does not fit on a single page. Because of this, it is not realistic to calculate the integrals from equation 2.24 manually. Luckily, this type of integral can be solved numerically by for example Mathematica[5]. Since all Grassman number have been removed from the equation, it is finally possible to take the limit where the integral actually is an integral, rather than a sum.

2.3 Numerical Analysis on the Four-Variable Correlation

To calculate a correlation function of two dimers, four Grassman variables are required. Take for example the correlation function of dimers (i, b) and $(i + 2r(\vec{a} + \vec{b}), b)$, with r integer. If the corresponding correlation function would be called $C(r)$ and would be independant of the original site i, as given in equation 2.25.

$$\begin{aligned} C(r) &= \langle \eta_{2m,2n} \bar{\eta}_{2m,2n+1} \eta_{2(m+r),2(n+r)} \bar{\eta}_{2(m+r),2(n+r)+1} \rangle \\ &= \langle \eta_{0,0} \bar{\eta}_{0,1} \eta_{2r,2r} \bar{\eta}_{2r,2r+1} \rangle \end{aligned} \tag{2.25}$$

The beauty of having calculated the correlation function for the two-variable case, is that it paves the way for any more-variable correlation functions, if combined with Wick's theorem. Applying Wick's theorem to equation 2.25 gives the following result:

$$C(r) = \langle \eta_{0,0} \bar{\eta}_{0,1} \rangle \langle \eta_{2r,2r} \bar{\eta}_{2r,2r+1} \rangle - \langle \eta_{0,0} \eta_{2r,2r} \rangle \langle \bar{\eta}_{0,1} \bar{\eta}_{2r,2r+1} \rangle + \langle \eta_{0,0} \bar{\eta}_{2r,2r+1} \rangle \langle \bar{\eta}_{0,1} \eta_{2r,2r} \rangle \tag{2.26}$$

The first term of equation 2.26 is two factors of 6. This makes sense, when realising that the correlation function of a single dimer (such as $\langle \eta_{0,0} \bar{\eta}_{0,1} \rangle$ and $\langle \eta_{2r,2r} \bar{\eta}_{2r,2r+1} \rangle$) is the same as the amount of possible coverings with one dimer fixed divided by all possible coverings without any fixed dimers. There are six ways to fix a dimer on each site, so there should six times more coverings if nothing is fixed.

The second term (with the minus-sign) is nil squared, independent of the distance r between the dimers. This is more intuitive, when realising that $\eta_{0,0}$ and $\eta_{2r,2r}$ have the same corresponding χ_p term, namely: $\chi_{\vec{p}}^1$. The product of this with itself is naught. The same holds true for $\bar{\eta}_{0,1}$, $\bar{\eta}_{2r,2r+1}$ and $\bar{\chi}_{\vec{p}}^3$, hence the nill squared.

If then the third term (which is dependant of r, unlike the first and second term) is given the name $f(r, r)$, equation can be rewritten to be:

$$C(r) = \frac{1}{36} + f(r, r) \tag{2.27}$$

---

[5]CHECK the sign of the exponent with mathematica

Computations in Mathematica, using equation 2.24, confirm the the $\left(\frac{1}{6}\right)^2$ and 0^2 terms. $f(r,r)$ has been put in Mathematica for different integer values of r. To inspect the general behaviour, the logarithm of the absolute value of $f(r,r)$ has been calculated for $r \in \{1,2,\ldots,16\}$,
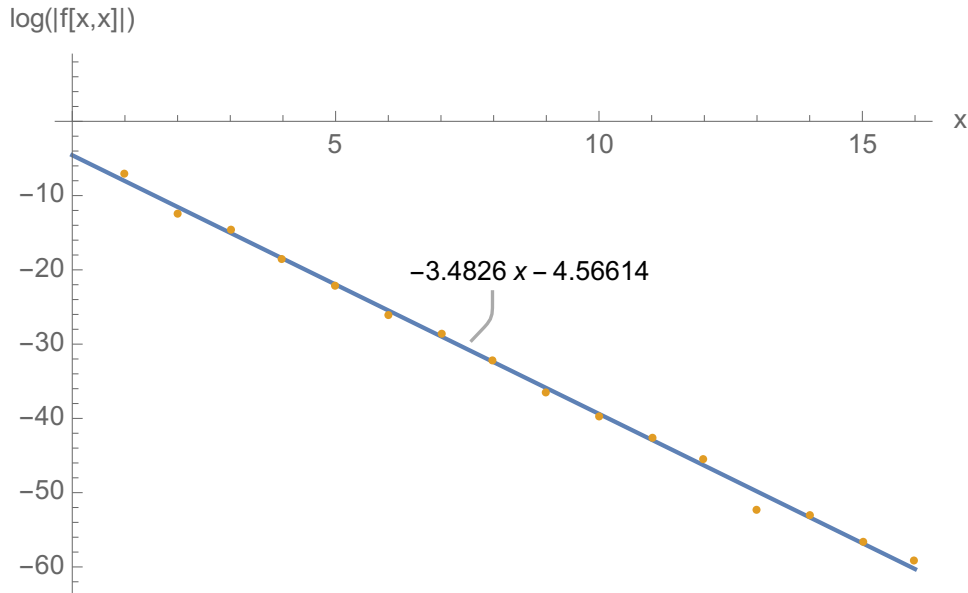
FIGURE 2.5: This figure shows the numerical result of the examination of $\log|f(x,x)|$ for $x \in \{1,2,\ldots,16\}$, graph made with Mathematica.

Figure 2.5 suggest a linear relation between $\log|f(r,r)|$ (y-axis) and r (x-axis): $y = -3.4826x - 4.56614$. The physical distance d between the dimers is $d = r \cdot a$, with a the lattice constant. Rewriting the linear formula in the form of exponential decay gives:

$$|f(r,r)| = 0.010e^{-3.48r}$$
$$|f(d)| = 0.010e^{-\frac{1.74}{a}d}$$
(2.28)

Following from equation 2.28 a correlation length of $\frac{a}{1.74}$ is found.

To conclude, even though the numerics in this section are not by any means definitive proof that correlation functions decay exponentially (plus $\frac{1}{36}$), it is consistent with earlier results[6] that show exponential decay. So, even without the calculations done in this chapter, this is enough evidence to assume the decay of the correlation is fast enough to be neglected in chapter 3.

---

[6]CHECK, I still need the reference for this

Chapter 3

Exact Ground State Solution of a Special Case of the Triangular RK-Hamiltonian

When considering the dimer model, it is normal to have states that are full coverings, with one dimer on every site. There would be an electron density n of one electron per site (so $n = 1$), or half-filling. A common way to add impurities to the model is to add doping of some sort. In the original paper[1] introducing the H_{RK}, these where single site holes: single unoccupied sites that were treated as spinless particles with positive charge, compared to half-filling. These particles decrease the electron density, so with a (negative) doping p: $n = 1 + p$.[2] Adding single electrons as impurities, rather than holes, gives a chargeless perturbation in spin that does not influence n.

An alternative idea is not to think in single-site perturbations, but in dimer perturbations. These dimers are a superposition of an electron (with spin $\pm\frac{1}{2}$) on one site and a hole on the other, and the other way around, as given in equation 3.1.

$$F^{\dagger}_{(i,\eta),\sigma} = \frac{c^{\dagger}_{i,\sigma} + c^{\dagger}_{i+\vec{\eta},\sigma}}{\sqrt{2}} \tag{3.1}$$

Here σ is the spin index, which will often be surpressed, unless specifically needed and (i, η) uses the same convention as for the Bosonic dimers (equation 1.14 and figure 1.2). This type of dimer is Fermionic, and will from here on be referred to as such. Similar to the Bosonic dimer, this dimer will be treated as a normal hard-core dimer, but then following anti-commutation rules, rather than commutation rules, as shown in equations 3.2 to 3.5. Keep in mind that Bosonic dimer operators always commute with Fermionic dimer operators.

$$\{F^{\dagger}_{i\sigma}, F^{\dagger}_{i'\sigma'}\} = 0 \tag{3.2}$$

$$\{F_{i\sigma}, F_{i'\sigma'}\} = 0 \tag{3.3}$$

$$\{F_{i\sigma}, F^{\dagger}_{i'\sigma'}\} = \delta_{ii',\sigma\sigma'} \tag{3.4}$$

$$F_{i\sigma}|0\rangle = 0 \tag{3.5}$$

---

[1] Rokhsar and Kivelson, 1988

[2] CHECK I want to make a comment on the behaviour w.r.t. the doping density

Adding Fermionic dimers to the system, naturally requires perturbations to the RK-Hamiltonian (equations 1.24 and 1.25) to investigate the changes due to the impurities. To keep these new terms local, and consistent with the way of thinking from the RK-Hamiltonian, all interactions will be given in terms of plaquettes: ⟋⟋ , ⟋⟋ , ▱ and ▱ . These are the relevant triangular plaquettes, where the red dimer represents the Fermion and the black dimer represents the Boson. This chapter will consider one specific perturbation: a perturbation that can be considered an extension of the RK-Point on the triangular lattice. The RK-Hamiltonian can be written down as in equation 3.7 and the perturbation is given in equation 3.8. The work done in the rest of this chapter will be very similar to the work that Feldmeier[3] has done on the square lattice.

$$H_p = H_{RK} + vH' \tag{3.6}$$

$$H_{RK} = v \sum \left(| \text{⟋⟋} \rangle - | \text{▱} \rangle \right) \left(\langle \text{⟋⟋} | - \langle \text{▱} | \right) \tag{3.7}$$

$$H' = \sum | \left(| \text{⟋⟋} \rangle + | \text{⟋⟋} \rangle - | \text{▱} \rangle - | \text{▱} \rangle \right) \left(\langle \text{⟋⟋} | + \langle \text{⟋⟋} | - \langle \text{▱} | - \langle \text{▱} | \right) \tag{3.8}$$

The Hamiltonian H_p in equation 3.6 is a sum of two projectors. Because of this, all eigenvalues have to be null, or larger. This is a property of the RK-point, it is an extension of the RK-point in the sense that it is a similar projection. Keep in mind that if all minus signs are changed to plus signs, the computation in section 3.1 could be executed the same way, with the main distinction being a minus sign here or there.

3.1   Finding the Ground State

Since H_p is a projector, the minimal eigenvalue is naturally naught, so by setting the energy to nil, a condition for the ground state can be found. To find this condition, it is useful to start by defining the state $|i_1, i_2\rangle = |(i_1, \eta_1), (i_2, \eta_2)\rangle$ as given below.

$$|(i_1, \eta_1), (i_2, \eta_2)\rangle = \frac{1}{\sqrt{N_t}} F^\dagger_{i_1, \eta_1} F^\dagger_{i_2, \eta_2} |0\rangle_{(i_1, \eta_1), (i_2, \eta_2)} \otimes \left(\sum_{c \in C_{(i_1, \eta_1), (i_2, \eta_2)}} |c\rangle \right) \tag{3.9}$$

Here $C_{(i_1, \eta_1), (i_2, \eta_2)}$ is the set of all subcoverings with dimers (i_1, η_1) and (i_2, η_2) empty, N_t is some constant, equal to the amount of possible dimer coverings without any sites left empty. Equation 3.9 is a good example of why using shorthand notation can be very useful. Since all subcoverings $|c\rangle$ are orthonormal, it is easy to find the magnitude of $|i_1, i_2\rangle$:

$$\begin{aligned} \langle i_1, i_2 | i_1, i_2 \rangle &= \frac{N_{i_1, i_2}}{N_t} \\ &= Q_c[i_1, i_2] \\ &= \langle i_1, i_2 \rangle_{classical} \end{aligned} \tag{3.10}$$

N_{i_1, i_2} is the amount of states with dimers i_1 and i_2 fixed (= the amount of subcoverings in C_{i_1, i_2}), $\langle i_1, i_2 \rangle_{classical}$ is the classical two-dimer correlation and $Q_c[i_1, i_2]$ is the

---

[3]Feldmeier, Huber, and Punk, 2018 and Feldmeier, 2018

notation used by Feldmeier[4], which will here be used for consistency. This entire chapter draws a lot from his work on the square lattice. Because of the $F_i^\dagger$ being Fermionic, $|i_1, i_2\rangle = -|i_2, i_1\rangle$, in addition to this: if the sets $\{i_1, i_2\}$ and $\{j_1, j_2\}$ are not the same, $\langle i_1, i_2 | j_1, j_2 \rangle = 0$.

Next, it is useful to define a state $|\phi_i\rangle$ on plaquette i as follows:

$$|\phi_i\rangle = | {\diagup\diagup} \rangle_i + | {\diagup\diagup} \rangle_i - | {\rule{1cm}{0cm}} \rangle_i - | {\rule{1cm}{0cm}} \rangle_i \tag{3.11}$$

Equation 3.11 can be used to define a projection operator P_i:

$$P_i = |\phi_i\rangle\langle\phi_i| \otimes \prod_{i' \neq i} id_{i'}$$

$$P_i(a) = \left(a|\phi_i\rangle\langle\phi_i| \right) \otimes \prod_{i' \neq i} id_{i'} \tag{3.12}$$

Which projects plaquette i on the state $|\phi_i\rangle$ (with prefactor a, if wanted) and keeps the rest of the system unchanged. Using this projector, equation 3.6 can be rewritten to:

$$H_p = H_{RK} + \sum_l P_l(v) \tag{3.13}$$

3.1.1 Using the Projector

Now that all preliminary objects have been defined, it is time to use the Hamiltonian, in the form of equation 3.13 on the state from equation 3.9. Even though this is a two-Fermion state, the calculation of ground states with a larger Fermionic doping should be done analogously. Since H_{RK} is at the RK-point, its contribution to the energy of $|i_1, i_2\rangle$ is naught. Hence:

$$H_p|i_1, i_2\rangle = 0 + \sum_l P_l(v)|i_1, i_2\rangle \tag{3.14}$$

Which reduces $H_p|i_1, i_2\rangle$ to only a sum over $P_l(v)|i_1, i_2\rangle$. For each dimer i there are four possible plaquettes of which the dimer i can be part. These plaquettes have been visualised in figure 3.1.

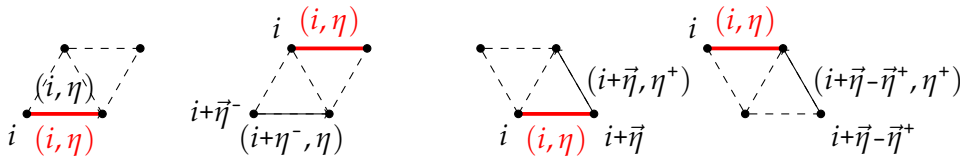FIGURE 3.1: This figure shows all plaquettes that contain the dimer (i, η), The plaquette index is given in black, along with the corresponding dimer. The η^+ and η^- are defined in equation 1.26 to 1.29

Using these plaquettes, $P_l(v)|i_1, i_2\rangle$ (where $l = (l, \xi)$) can be rewritten to:

---

[4]Chapter 4 from Feldmeier, 2018 is dedicated to the same subject on the square lattice

$$P_l(v)|i_1, i_2\rangle = \sum_{k=1}^{2} \left(\delta_{l i_k} \delta_{\xi \eta_k} + \delta_{l, i_k + \vec{\eta}_k^-} \delta_{\xi \eta_k} + \delta_{l, i_k + \vec{\eta}_k} \delta_{\xi \eta_k^+} + \delta_{l, i_k + \vec{\eta}_k - \vec{\eta}_k^+} \delta_{\xi \eta_k^+} \right) P_l(v)|i_1, i_2\rangle$$

(3.15)

This expression has 8 $\delta\delta$ terms that need to be considered. Take the term with $\delta_{l i_1} \delta_{\xi \eta_1}$ to begin with. Because of the the multiplication Kronecker delta, the factor $|(i_1, \eta_1), (i_2, \eta_2)\rangle$ can be written as $|(l, \xi), (i_2, \eta_2)\rangle$. The operator $F_{(l,\xi)}^\dagger$ is part of $|(l, \xi), (i_2, \eta_2)\rangle$, because of this, the only term that is not zero after $P_{(l,\xi)}(v)$ has worked on it is:

$$P_{(l,\xi)}(v)|(l,\xi),(i_2,\eta_2)\rangle = \frac{1}{\sqrt{N_t}} P_{(l,\xi)}(v) \left(F_{(l,\xi)}^\dagger F_{(i_2,\eta_2)}^\dagger D_{(l-\vec{\xi}^-,\xi)}^\dagger |0\rangle_{()()()} \right) \otimes \left(\sum_{c' \in C_{()()()}} |c'\rangle \right)$$

(3.16)

Here $()()()= (l, \xi)(i_2, \eta_2)(l - \vec{\xi}^-, \xi)$, to avoid a terrible mess of notation. Bosonic and Fermionic operators commute, so $F^\dagger F^\dagger D^\dagger = F^\dagger D^\dagger F^\dagger$. Then $P_{(l,\xi)}(v)$ acts on plaquette (l, ξ) as follows:

$$P_{(l,\xi)}(v) F_{(l,\xi)}^\dagger D_{(l-\vec{\xi}^-,\xi)}^\dagger |0\rangle_{l,\eta} = v |\phi_{l,\xi}\rangle \langle \phi_{l,\xi} | F_{(l,\xi)}^\dagger D_{(l-\vec{\xi}^-,\xi)}^\dagger |0\rangle_{l,\eta}$$
$$= v \cdot (-1) |\phi_{l,\xi}\rangle$$

(3.17)

The minus sign comes from the minus sign for horizontal dimers in equation 3.11. Using all this, the result is:

$$\delta_{l i_1} \delta_{\xi \eta_1} P_l(v)|i_1, i_2\rangle = -\frac{v \delta_{l i_1} \delta_{\xi \eta_1}}{\sqrt{N_t}} |\phi_{l,\xi}\rangle \otimes F_{i_2,\eta_2}^\dagger |0\rangle_{(i_2,\eta_2)} \otimes \left(\sum_{c' \in C_1^3} |c'\rangle \right)$$

(3.18)

In which C_1^3 is even shorter notation for $C_{(l,\xi)(i_2,\eta_2)(l-\vec{\xi}^-,\xi)}$. All steps that took the $\delta_{l i_1} \delta_{\xi \eta_1}$-term from equation 3.15 to equation 3.18 can be applied to all other $\delta\delta$-terms. For all i_1 terms, the results are given in equation 3.19 to 3.21.

$$\delta_{l, i_1 + \vec{\eta}_1^-} \delta_{\xi \eta_1} P_l(v)|i_1, i_2\rangle = -\frac{v \delta_{l, i_1 + \vec{\eta}_1^-} \delta_{\xi \eta_1}}{\sqrt{N_t}} |\phi_{l,\xi}\rangle \otimes F_{i_2,\eta_2}^\dagger |0\rangle_{(i_2,\eta_2)} \otimes \left(\sum_{c' \in C_2^3} |c'\rangle \right) \quad (3.19)$$

$$\delta_{l, i_1 + \vec{\eta}_1} \delta_{\xi \eta_1^+} P_l(v)|i_1, i_2\rangle = \frac{v \delta_{l, i_1 + \vec{\eta}_1} \delta_{\xi \eta_1^+}}{\sqrt{N_t}} |\phi_{l,\xi}\rangle \otimes F_{i_2,\eta_2}^\dagger |0\rangle_{(i_2,\eta_2)} \otimes \left(\sum_{c' \in C_3^3} |c'\rangle \right) \quad (3.20)$$

$$\delta_{l, i_1 + \vec{\eta}_1 - \vec{\eta}_1^+} \delta_{\xi \eta_1^+} P_l(v)|i_1, i_2\rangle = \frac{v \delta_{l, i_1 + \vec{\eta}_1 - \vec{\eta}_1^+} \delta_{\xi \eta_1^+}}{\sqrt{N_t}} |\phi_{l,\xi}\rangle \otimes F_{i_2,\eta_2}^\dagger |0\rangle_{(i_2,\eta_2)} \otimes \left(\sum_{c' \in C_4^3} |c'\rangle \right) \quad (3.21)$$

Where $C_2^3 = C_{(i_2,\eta_2)(l,\xi)(l-\vec{\xi}^-,\xi)}$ and $C_3^3 = C_4^3 = C_{(i_2,\eta_2)(l-\vec{\xi}^-+\vec{\xi},\xi^-)(l-\vec{\xi}^-,\xi^-)}$. Since these are the sets of all subcoverings that do not cover the subscripted dimers, the order of these dimers does not matter, but more important both the pair (l, ξ) and $(l - \vec{\xi}^-, \xi)$ and the pair $(l - \vec{\xi}^- + \vec{\xi}, \xi^-)$ and $(l - \vec{\xi}^-, \xi^-)$ cover the same four sites. Namely the four sites of the plaquette with index (l, ξ). Hence, $C_n^3 = C_{()()()}$ of all n. Because of

this, it is useful to introduce yet another new notation, as this shortens the expressions in equation 3.18 to 3.21 significantly:

$$|\phi_{l,\xi}, (i_k, \eta_k)\rangle_0 = |\phi_{l,\xi}\rangle \otimes F^\dagger_{i_k,\eta_k} |0\rangle_{(i_k,\eta_k)} \otimes \left(\sum_{c' \in C_{()()()}} |c'\rangle \right) \tag{3.22}$$

With the knowledge that $|i_1, i_2\rangle = -|i_2, i_1\rangle$ holds, one easily finds that the values of all $\delta\delta$ terms with i_2 are equal to their i_1 counterparts, but then with a minus sign, and with i_1 and i_2 swapped. This combines with equation 3.22 to equation 3.23.

$$P_l(v)|i_1, i_2\rangle =$$
$$v \sum_{k=1}^{2} \frac{(-1)^k}{\sqrt{N_t}} \left(\delta_{li_k}\delta_{\xi\eta_k} + \delta_{l,i_k+\vec{\eta}_{\bar{k}}}\delta_{\xi\eta_k} - \delta_{l,i_k+\vec{\eta}_k}\delta_{\xi\eta_k^+} - \delta_{l,i_k+\vec{\eta}_k-\vec{\eta}_k^+}\delta_{\xi\eta_k^+} \right) |\phi_{l,\xi}, (i_{\bar{k}}, \eta_{\bar{k}})\rangle_0 \tag{3.23}$$

Note that $i_{\bar{k}}$ represents the complement of i_k ($\bar{k} = 2$ fo $k = 1$, etc.). This formula can be generalised to more-dimer systems: the 2 would be replaced by the amount of dimers n, and $(i_{\bar{k}}, \eta_{\bar{k}})$ would be replaced by $\{(i_{\bar{k}}, \eta_{\bar{k}})\}$, the set of all dimers but i_k.

Next, define a variety on equation 3.22 (more-dimer version can be defined analogously):

$$|\phi_{l,\xi}, (i_k, \eta_k)\rangle = \frac{1}{\sqrt{N_{(l,\xi)(l-\vec{\xi}^-,\xi)(i_k,\eta_k)}}} |\phi_{l,\xi}, (i_k, \eta_k)\rangle_0 \tag{3.24}$$

This definition is chosen, such that equation 3.23 can be rewritten to:

$$P_l(v)|i_1, i_2\rangle = v \sum_k (-1)^k \sqrt{Q_c[(l,\xi), (l-\vec{\xi}^-,\xi), (i_k,\eta_k)]} \left(\sum \delta\delta \right) |\phi_{l,\xi}, (i_{\bar{k}}, \eta_{\bar{k}})\rangle \tag{3.25}$$

Not that $Q_c[(l,\xi), (l-\vec{\xi}^-,\xi), (i_k,\eta_k)]$ is null if there is any overlap between the fixed dimers, this ensures that this formula holds, even when (i_1, η_1) and (i_2, η_2) are (partially) in the same plaquette.

3.1.2 Proposing a Ground State

Knowing how $|i_1, i_2\rangle$ responds to the Hamiltonian, introduces an opportunity in creating a ground state, built from these two-Fermion states. This state will be as general as possible, for a two-Fermion state, namely: a linear superposition of all possibilities. The state that eventually will become the ground state is defined as:

$$|\psi_0\rangle = \sum_{i_1, i_2} A_{i_1,i_2} |i_1, i_2\rangle \tag{3.26}$$

When using $H_p = \sum_l P_l(v)$ on $|\psi_0\rangle$, the result is:

$$H_p|\psi_0\rangle = v \sum_{l,i_1,j_2,k} (-1)^k \sqrt{Q_c[\dots]} \left(\sum \delta\delta A_{i_k} \right) |\phi_{l,\xi}, (i_{\bar{k}}, \eta_{\bar{k}})\rangle \tag{3.27}$$

Since $\sum_{i_1,i_2}$ runs twice over all possible dimers, The distinction between in the indices in $|\phi_{l,\xi}, (i_{\bar{k}}, \eta_{\bar{k}})\rangle$ becomes somewhat meaningless. It is more useful to look at each $|\phi_{l,\xi}, (i, \eta)\rangle$ and look what its prefactor is.

The sum over l (and ξ) is conserved, but the sum over i_k (and η_k) fix A. In short notation, the sum over i_1 turns all indices i_1 in the $\delta\delta$ part into l -terms for A: $\sum A_{l,i_2}$. Similarly, the sum over i_2 results in $A_{i_1,l}$. So, renaming the remaining sums over i_k simply to i gives:

$$\sum \delta\delta A_{i_k} = - A_{(l,\xi)(i,\eta)} - A_{(l-\vec{\xi}^-,\xi)(i,\eta)} + A_{(l-\vec{\xi}^-,\xi^-)(i,\eta)} + A_{(l-\vec{\xi}^-+\vec{\xi},\xi^-)(i,\eta)}$$
$$+ A_{(i,\eta)(l,\xi)} + A_{(i,\eta)(l-\vec{\xi}^-,\xi)} - A_{(i,\eta)(l-\vec{\xi}^-,\xi^-)} - A_{(i,\eta)(l-\vec{\xi}^-+\vec{\xi},\xi^-)} \tag{3.28}$$

Using equation 3.28, together the beforehand described resummation, turns equation 3.27 into:

$$H_p|\psi_0\rangle = v \sum_{l,i} \sqrt{Q_c[\ldots]} \left(\sum \delta\delta A_{i_k} \right) |\phi_{l,\xi}, (i, \eta)\rangle \tag{3.29}$$

Here, $Q_c[\ldots] = Q_c[(l, \xi), (l - \vec{\xi}^-, \xi), (i, \eta)]$, as before. The next step is to find an expression for the energy in terms of A:

$$\langle\psi_0|H_p|\psi_0\rangle = v \sum_{i_1,i_2,j_1,j_2,l} A^*_{j_1,j_2} A_{i_1,i_2} \langle j_1, j_2|\phi_l\rangle\langle\phi_l|i_1, i_2\rangle$$
$$= v \sum_{l,i} Q_c[(l, \xi), (l - \vec{\xi}^-, \xi), (i, \eta)] \left| \sum \delta\delta A_{i_k} \right|^2 \tag{3.30}$$

If $\langle\psi_0|H_p|\psi_0\rangle$ is to be nil, that means all $\sum \delta\delta A_{i_k}$ need to be nil. To find a solution for A, choose:

$$A_{i_1,i_2} = a_{i_1} b_{i_2} \tag{3.31}$$

This definition reduces $\sum \delta\delta A_{i_k} = 0$ to:

$$0 = b_{i,\eta} \left(- a_{l,\xi} - a_{l-\vec{\xi}^-,\xi} + a_{l-\vec{\xi},\xi^-} + a_{l-\vec{\xi}^-+\vec{\xi},\xi^-} \right)$$
$$- a_{i,\eta} \left(- b_{l,\xi} - b_{l-\vec{\xi}^-,\xi} + b_{l-\vec{\xi},\xi^-} + b_{l-\vec{\xi}^-+\vec{\xi},\xi^-} \right) \tag{3.32}$$

This is a very symmetric expression, which is useful, because that suggests to treat both lines from equation 3.32 separately. Now, it is possible to mathematically prove that the solution $a_{i,\eta} = 0 = b_{i,\eta}$ is a rather boring solution. Jokes aside, looking for a solution for $-a_{l,\xi} - a_{l-\vec{\xi}^-,\xi} + a_{l-\vec{\xi},\xi^-} + a_{l-\vec{\xi}^-+\vec{\xi},\xi^-} = 0$ and the equivalent $-b_{l,\xi} - b_{l-\vec{\xi}^-,\xi} + b_{l-\vec{\xi},\xi^-} + b_{l-\vec{\xi}^-+\vec{\xi},\xi^-} = 0$ can be done by making the following Ansatz:

$$a_{i,\eta} = c_{i,\eta}(\vec{p}_1) = C(\vec{p}_1)_\eta e^{i\vec{p}_1 \cdot \vec{i}} \tag{3.33}$$
$$b_{i,\eta} = c_{i,\eta}(\vec{p}_2) = C(\vec{p}_2)_\eta e^{i\vec{p}_2 \cdot \vec{i}} \tag{3.34}$$

Filling in this new definition in either of the terms between brackets from equation 3.32 set equal to zero gives:

$$C_\eta(\vec{p}_k) = \frac{1 + e^{i\vec{p}_k \cdot \vec{\eta}}}{1 + e^{i\vec{p}_k \cdot \vec{\eta}^-}} C_{\eta^-}(\vec{p}_k) \tag{3.35}$$

By applying the definition of the η^- multiple times, it can be found that $C_\eta(p) = C_{((\eta^-)^-)^-}(p)$, which is good, because $\eta = ((\eta^-)^-)^-$. After this small legitimacy check, $C_\eta(p)$ can fully be defined:

$$C_\eta(p) = \frac{q}{\sqrt{N}} \frac{1 + e^{i\vec{p}_k \cdot \vec{\eta}}}{|1 + e^{i\vec{p}_k \cdot \vec{\eta}}|^2 + |1 + e^{i\vec{p}_k \cdot \vec{\eta}^-}|^2 + |1 + e^{i\vec{p}_k \cdot \vec{\eta}^+}|^2} \tag{3.36}$$

Equation 3.36 is chosen as it is, because now $|C_\eta|^2 + |C_{\eta^-}|^2 + |C_{\eta^+}|^2 = \frac{q^2}{N}$. N is the number of sites, and q will later prove to be $q = \sqrt{6}$. With this definition, and previous definitions 3.33, 3.34 and 3.31, it is possible to write $|\psi_0\rangle = |p_1, p_2\rangle$ as:

$$|p_1, p_2\rangle = \sum_{i_1, \eta_1, i_2, \eta_2} C_{\eta_1}(p_1) C_{\eta_2}(p_2) e^{i(\vec{p}_1 \cdot \vec{i}_1 + \vec{p}_2 \cdot \vec{i}_2)} |(i_1, \eta_1), (i_2, \eta_2)\rangle \tag{3.37}$$

3.1.3 Normalising the Ground State

The last thing to do, before $|p_1, p_2\rangle$ can be considered a proper ground state, is normalising it. In other words, it is necessary to find a value for q that normalises the state.

$$\begin{aligned}
\langle p_1, p_2 | p_1, p_2 \rangle &= \sum_{i_1, i_2, j_1, j_2} a_{i_1}^* b_{i_2}^* a_{j_1} b_{j_2} \langle i_1, i_2 | j_1, j_2 \rangle \\
&= \sum_{i_1, i_2, j_1, j_2} a_{i_1}^* b_{i_2}^* a_{j_1} b_{j_2} \left(\delta_{i_1 j_1} \delta_{i_2 j_2} - \delta_{i_1 j_2} \delta_{i_2 j_1} \right) Q_c[i_1, i_2] \\
&= \sum_{i_1, i_2} \left(|a_{i_1}|^2 |b_{i_2}|^2 - a_{i_1}^* a_{i_2} b_{i_2}^* b_{i_1} \right) Q_c[i_1, i_2]
\end{aligned} \tag{3.38}$$

Since the first term of that last line is straightforward, the second term is investigated first:

$$\text{term } 2 = \sum_{\eta_1, \eta_2} C_{\eta_1}^*(p_1) C_{\eta_2}^*(p_2) C_{\eta_2}(p_1) C_{\eta_1}(p_2) \sum_{i_1, i_2} e^{i(\vec{i}_1 - \vec{i}_2) \cdot (\vec{p}_2 - \vec{p}_1)} Q_c[(i_1, \eta_1), (i_2, \eta 2)] \tag{3.39}$$

The last part of term 2 can be seen as a Fourier transform of a classical two-dimer correlation. As the entirety of chapter 2 is trying to show[5], the classical two dimer correlation has the form:

$$Q_c(r) = \frac{1}{36} + \mathcal{O}(e^{-\lambda|r|}) \tag{3.40}$$

---

[5]This remark is the entire reason there is a chapter two in the first place, the calculation got a bit out of hand CHECK: other reference to this?

Here r is the distance between the two dimers and λ is an unimportant (for this derivation) positive real constant. For large lattices, on average $r \to \infty$, so the exponent becomes negligible in a Fourier transform. Taking a Fourier transform over $\frac{1}{36}$ gives a Kronecker delta $\delta_{\vec{p}_2 - \vec{p}_1}$, which is always null, unless the two momenta $\vec{p}_1$ and $\vec{p}_2$ are equal. But the state $|p_1, p_2\rangle$ is zero in that case, so this term is null. Note that taking a Fourier transform only requires one summation over i_1 or i_2, the other summation remains and gives a factor of order N. But in both cases this is irrelevant because of faster (exponential) decay or a factor nil (the delta).

Now that the second term has been shown to be null, it is time to look at the first term (while keeping equation 3.40 in mind):

$$\langle p_1, p_2 | p_1, p_2 \rangle = \sum_{i_1, i_2} \sum_{\eta_1} |C_{\eta_1}|^2 \sum_{\eta_2} |C_{\eta_2}|^2 \left(\frac{1}{36} + \mathcal{O}(e^{-\lambda |r|}) \right) \tag{3.41}$$

The exponent will go fast to zero, again, so:

$$\langle p_1, p_2 | p_1, p_2 \rangle = \sum_{i_1, i_2} \frac{q^2}{N} \frac{q^2}{N} \frac{1}{36} = \frac{q^4}{36} \tag{3.42}$$

Which finally shows that with $q = \sqrt{6}$, $|p_1, p_2\rangle$ is a normalised ground state of H_p, with zero energy.

3.2   Using the Ground State

To learn more about the ground state discovered in section 3.1, one can tweak the Hamiltonian and see how the energy responds to that in first order of perturbation theory. The difference in energy ΔE is given by:

$$\Delta E = \langle \Psi_0 | \Delta H | \Psi_0 \rangle \tag{3.43}$$

In this expression, Ψ_0 is the original unperturbed ground state of the original Hamiltonian ($|p_1, p_2\rangle$ and H_p, respectively), and ΔH is the perturbation on the Hamiltonian. Since the energy of $|p_1, p_2\rangle$ is nil, the energy of the perturbed Hamiltonian (up to first order) will be equal to exactly ΔE.

3.2.1   First Order Perturbation to the Ground State

The perturbations that will be considered in this section are dimer swaps. This could mean a plaquette flip (rotation by $180°$, not by $90°$), but also a swap of two dimers over longer distance. Call the type of operation a u-swap[6], with the corresponding Hamiltonian:

$$\Delta H_u = -\delta_u \sum_{s=1}^{S_u} \sum_{j,\zeta} F^\dagger_{j + r_u^{s,\zeta}, \zeta + \eta_u^{s,\zeta}} D^\dagger_{j,\zeta} D_{j + r_u^{s,\zeta}, \zeta + \eta_u^{s,\zeta}} F_{j,\zeta} \tag{3.44}$$

---

[6]Section 4.3 from Feldmeier, 2018 calls this t_i

In which $r_u^{s,\zeta}$ and $\eta_u^{s,\zeta}$ are the difference in position and orientation between the two dimers that an u-swap consists of. The index s goes over all S_u ways that a dimer (j, ζ) can perform a u-swap. Lastly, δ_u is the energy attributed to said u-swap. Next up is finding an expression for $\Delta E = \langle p_1, p_2 | \Delta H | p_1, p_2 \rangle$:

$$\Delta E = -\delta_u \sum_{s,j,\zeta} \sum_{i_1,i_2,l_1,l_2} a_{l_1}^* b_{l_2}^* a_{i_1} b_{i_2} \langle l_1, l_2 | F_{j+r_u^{s,\zeta}, \zeta+\eta_u^{s,\zeta}}^\dagger D_{j,\zeta}^\dagger D_{j+r_u^{s,\zeta}, \zeta+\eta_u^{s,\zeta}} F_{j,\zeta} | i_1, i_2 \rangle \tag{3.45}$$

Indices have been kept short, where possible, and in the next few lines all orientations will be suppressed, until new orientations arise that have not yet been written down. Thus:

$$\langle l_1, l_2 | F^\dagger D^\dagger D F | i_1, i_2 \rangle = \delta_{ji_1} \left(\delta_{l_1, j+r_u^{s,\zeta}} \delta_{l_2 i_2} - \delta_{l_2, j+r_u^{s,\zeta}} \delta_{l_1 i_2} \right) Q_c[i_1, i_2, i_1 + r_u^{s,\zeta}]$$
$$+ \delta_{ji_2} \left(\delta_{l_2, j+r_u^{s,\zeta}} \delta_{l_1 i_1} - \delta_{l_1, j+r_u^{s,\zeta}} \delta_{l_2 i_1} \right) Q_c[i_1, i_2, i_2 + r_u^{s,\zeta}] \tag{3.46}$$

Taking the sum over j removes the Kronecker deltas outside the brackets, without changing the a and b factors, and ir turns $r_u^{s,\zeta}$ into r_u^{s,η_k} ($i_k = (i_k, \eta_k)$). Then, after taking the sums over both l_1 and l_2, the result is:

$$\Delta E = -\delta_u \sum_{s,i_1,i_2} a_{i_1} b_{i_2} \left(\left(a_{i_1+r_u^{s,\eta_1}}^* b_{i_2}^* - a_{i_2}^* b_{i_1+r_u^{s,\eta_1}}^* \right) Q_c[i_1, i_2, i_1 + r_u^{s,\eta_1}] \right.$$
$$\left. + \left(a_{i_1}^* b_{i_2+r_u^{s,\eta_2}}^* - a_{i_2+r_u^{s,\eta_2}}^* b_{i_1}^* \right) Q_c[i_1, i_2, i_1 + r_u^{s,\eta_2}] \right) \tag{3.47}$$

Rename the terms to: $\Delta E = -\delta_u \sum \sum (T_1 + T_2 + T_3 + T_4)$, and treat them individually, beginning with T_1 and filling in the C-terms for a and b:

$$T_1 = \sum_{s,i_1,i_2} |C_{\eta_2}(p_2)|^2 C_{\eta_1}(p_1) C_{\eta_1 + \eta_u^{s,\eta_1}}(p_1) e^{-i r_u^{s,\eta_1} \cdot \vec{p}_1} Q_c[i_1, i_2, i_1 + r_u^{s,\eta_1}] \tag{3.48}$$

This term contains[7]:

$$\sum_{i_2, \eta_2} |C_{\eta_2}(p_2)|^2 Q_c[i_1, (i_2, \eta_2), i_1 + r_u^{s,\eta_1}] = Q_c[i_1, i_1 + r_u^{s,\eta_1}] \tag{3.49}$$

Which is independent of the position i_1 because $r_u^{s,\eta}$ is relative, so $Q_c[i_1, i_1 + r_u^{s,\eta_1}] = Q_c[(0, \eta_1), r_u^{s,\eta_1}]$. Because of this, after taking the sum over i_1 and filling in the C-terms even further and writing $\eta_1 = \eta$, the result is:

$$T_1 = -6\delta_u \sum_{s,\eta} \frac{(1 + e^{i\vec{p}_1 \cdot \vec{\eta}})(1 + e^{-i\vec{p}_1 \cdot (\vec{\eta} + \vec{\eta}_u^{s,\eta})}) e^{-i\vec{p}_1 \cdot \vec{\eta}_u^{s,\eta}}}{|1 + e^{i\vec{p}_1 \cdot \vec{\eta}}|^2 + |1 + e^{i\vec{p}_1 \cdot \vec{\eta}^-}|^2 + |1 + e^{i\vec{p}_1 \cdot \vec{\eta}^+}|^2} Q_c[(0, \eta), (r_u^{s,\eta}, \eta + \eta_u^{s,\eta})]$$
$$= \varepsilon(p_1) \tag{3.50}$$

---

[7] CHECK I do not believe this is correct, but Johannes used it

The term T_3 is similar to T_1, but with the following variables swapped: $i_1 \leftrightarrow i_2$ and $a \leftrightarrow b$ or $p_1 \leftrightarrow p_2$. This results via the same logic in:

$$T_3 = \varepsilon(p_2) \tag{3.51}$$

When filling in the the definitions of a, b and then C in T_2, it will be of the form:

$$T_2 = \delta_u \sum_s \sum_{\eta_1, \eta_2} C_{\eta_1}(p_1) C_{\eta_2}(p_2) C^*_{\eta_2}(p_1) C^*_{\eta_1 + \eta_u^{s, \eta_1}}(p_2) e^{-i \vec{p}_2 \cdot r_u^{s, \eta_1}}$$
$$\times \sum_{i_1, i_2} e^{i(\vec{i}_1 - \vec{i}_2)(\vec{p}_1 - \vec{p}_2)} Q_c[i_1, i_2, i_2 + r_u^{s, \eta_1}] \tag{3.52}$$

Of which only the second line is relevant: it contains a Fourier transform of a correlation function. Similar to equation 3.40, this is again the sum of some constant and an exponential decay. So this term too (and with it the very similar T_4), will be null, for large lattices:

$$T_2 = 0 = T_4 \tag{3.53}$$

If one finally combines all terms T_i the final result for the first order perturbation in the energy is obtained:

$$\Delta E = \varepsilon(p_1) + \varepsilon(p_2) \tag{3.54}$$

This derivation can be repeated similarly for more-particle systems. The corresponding energy is given below.

$$\Delta E = \sum_i \varepsilon(p_i) \tag{3.55}$$

3.2.2 Quasi-Particle Approach

Since the energy (equation 3.54 and 3.55) of the ground state (equation 3.37) of H_p (equation 3.6) is a sum of separate energies $\varepsilon(p_i)$ corresponding to a single momentum, these energies can be treated as single-quasi-particle excitations of the RK-Hamiltonian. To do so, let $|0^*\rangle = |RK\rangle$, the ground state of the non-Fermionic RK-Hamiltonian. Then a state $|p_1, \ldots, p_n\rangle$ can be described as follows:

$$|p_1, \ldots, p_n\rangle = \prod_i f^\dagger_{p_i} |0^*\rangle \tag{3.56}$$

$$f^\dagger_p = \sum_{i, \eta} C_\eta(p) e^{i\vec{p} \cdot \vec{i}} F^\dagger_{i\eta} D_{i\eta} \tag{3.57}$$

$$H_p |p_1, \ldots, p_n\rangle = \sum_i \varepsilon(p_i) \tag{3.58}$$

Because of equation 3.58, it makes sense to want to write H_p in terms of f-operators:

$$H_p = \sum_p \varepsilon(p) f_p^\dagger f_p \qquad (3.59)$$

But for this to make sense, $f_p^\dagger$ needs to be a properly Fermionic operator that follows the anti-commutation relations:

$$\{f_p, f_q\} = 0 \qquad (3.60)$$
$$\{f_p^\dagger, f_q^\dagger\} = 0 \qquad (3.61)$$
$$\{f_p, f_q^\dagger\} \overset{?}{=} \delta_{pq} \qquad (3.62)$$

The first two are no problem, but the last one gives some complications. Using that $C_\eta(p)e^{i\vec{p}\cdot\vec{i}} = a_{i\eta}(p)$:

$$
\begin{aligned}
\{f_{p_1}, f_{p_2}^\dagger\} &= \sum_{i_1, i_2} a_{i_1}(p_1) a_{i_2}^*(p_2) \{F_{i_1}^\dagger D_{i_1}, D_{i_2}^\dagger F_{i_2}\} \\
&= \sum_{i_1, i_2} a_{i_1}(p_1) a_{i_2}^*(p_2) \delta_{i_1 i_2} \left(F_{i_1}^\dagger F_{i_2} + D_{i_2}^\dagger D_{i_1}\right) \qquad (3.63) \\
&= \sum_{i_1} a_{i_1}(p_1) a_{i_1}^*(p_2) \hat{N}_{i_1}
\end{aligned}
$$

In which $\hat{N}_i = F_i^\dagger F_i + D_i^\dagger D_i$, the operator that counts the amount of dimers (both Fermionic and Bosonic) of type $i = (i, \eta)$. Evidently, this is not nil, at all. Luckily, taking the absolute value (squared) of $\{f_{p_1}, f_{p_2}^\dagger\}|0^*\rangle$ gives something more useful after writing all a-terms as C and after realising $\langle 0 * | \hat{N}_{i_1, \eta_1} N_{i_2, \eta_2} |0^*\rangle = Q_c[(i_1, \eta_1), (i_2, \eta_2)]$:

$$
\begin{aligned}
|\{f_{p_1}, f_{p_2}^\dagger\}|0^*\rangle|^2 &= \sum_{\eta_1, \eta_2} C_{\eta_1}(p_1) C_{\eta_1}^\dagger(p_2) C_{\eta_2}^*(p_1) C_{\eta_2}(p_2) \\
&\qquad \times \sum_{i_1, i_2} e^{i(\vec{i}_1 - \vec{i}_2)\cdot(\vec{p}_1 - \vec{p}_2)} Q_c[(i_1, \eta_1), (i_2, \eta_2)] \quad (3.64)
\end{aligned}
$$

The two-dimer correlation can be approximated by equation 3.40 for large lattices. After one sum over i_2 the result is:

$$
\begin{aligned}
|\{f_{p_1}, f_{p_2}^\dagger\}|0^*\rangle|^2 &= \sum_{\eta_1, \eta_2} C_{\eta_1}(p-1) C_{\eta_1}^\dagger(p_2) C_{\eta_2}^*(p_1) C_{\eta_2}(p_2) \\
&\qquad \times \sum_{i_1} e^{i(\vec{i}_1)\cdot(\vec{p}_1 - \vec{p}_2)} \left(\frac{N}{36}\delta_{p_1, p_2} + \mathcal{O}(e^{-\lambda|r|})\right) \quad (3.65)
\end{aligned}
$$

Which after neglecting the exponent, taking the sum over i_1 and keeping the Kronecker delta in mind gives:

$$|\{f_{p_1}, f_{p_2}^\dagger\}|0^*\rangle|^2 = \sum_{\eta_1, \eta_2} C_{\eta_1}(p_1) C_{\eta_1}^\dagger(p_1) C_{\eta_2}^*(p_1) C_{\eta_2}(p_1) \frac{N^2}{36} \delta_{p_1 p_2}$$
$$= \frac{36}{N^2} \frac{N^2}{36} \delta_{p_1 p_2} = \delta_{p_1 p_2} \tag{3.66}$$

This is obviously not enough to be able to say that the operator is perfectly Fermionic.

3.2.3 Difference Between Square and Triangular Lattice

Up until here, this entire chapter has roughly followed the same calculation as done by Feldmeier in chapter 4 his master thesis[8], who worked on the square lattice. Even though doing calculations the triangular lattice is more convoluted and tedious, especially when it comes to notation, the physics described up until here are the same for both cases. The next step on the square lattice would be to constrain the system to one topological sector and then find a constraint for which equation 3.62 does hold. For the square lattice, this condition is that $p_x = p_y$, but when repeating that same process on the triangular lattice the momenta for which the operator $f_p^\dagger$ is properly Fermionic is given by:

$$\vec{p} \cdot \vec{\eta} = \vec{p} \cdot \vec{\eta}^- \tag{3.67}$$

On first glance this seems fine, until the realisation kicks in that this needs to hold for all η. So by extension:

$$\vec{p} \cdot \vec{\eta} = \vec{p} \cdot \vec{\eta}^- = \vec{p} \cdot \vec{\eta}^+ \tag{3.68}$$

And that's where it gets troublesome. Now, in principle one could vind the values of p_1 and p_2 for which the following holds:

$$\begin{aligned} 0 = \quad & \left(1 + e^{i\vec{p}_1 \cdot \vec{\eta}^-}\right)\left(1 + e^{-i\vec{p}_2 \cdot \vec{\eta}^-}\right)\left(1 + e^{i(\vec{p}_1 - \vec{p}_2) \cdot \vec{\eta}}\right) \\ & - \left(1 + e^{i\vec{p}_1 \cdot \vec{\eta}}\right)\left(1 + e^{-i\vec{p}_2 \cdot \vec{\eta}}\right)\left(1 + e^{i(\vec{p}_1 - \vec{p}_2) \cdot \vec{\eta}^-}\right) \end{aligned} \tag{3.69}$$

This needs to hold for all η. This does hold when $p_1 = 0$ or $p_2 = 0$, but that does not really give a proper space on which to work.

Anyways, for the strange shaped space on which it does work, it is possible to relate $f_p^\dagger$ to the electron operators. In terms of Dimer operators, the electron annihilator can be written as:

$$c_{i\alpha} = \frac{\epsilon_{\alpha\beta}}{\sqrt{6}} \sum_{\eta} \left(F_{i,\eta,\beta}^\dagger D_{i,\eta} + F_{i-\vec{\eta},\eta,\beta}^\dagger D_{i-\vec{\eta},\eta} \right) \tag{3.70}$$

Or in terms of momentum:

---

[8]Feldmeier, 2018

$$
\begin{aligned}
c_{p\alpha} &= \frac{1}{\sqrt{N}} \sum_i e^{i\vec{p}\cdot\vec{i}} c_{i\alpha} \\
&= \frac{\epsilon_{\alpha\beta}}{\sqrt{6N}} \sum_{i,\eta} e^{i\vec{p}\cdot\vec{i}} \left(F^\dagger_{i,\eta,\beta} D_{i,\eta} + F^\dagger_{i-\vec{\eta},\eta,\beta} D_{i-\vec{\eta},\eta} \right) \\
&= \frac{\epsilon_{\alpha\beta}}{\sqrt{6N}} \sum_{i,\eta} e^{i\vec{p}\cdot\vec{i}} \left(1 + e^{-i\vec{p}\cdot\vec{\eta}} \right) F^\dagger_{i,\eta,\beta} D_{i,\eta}
\end{aligned}
\tag{3.71}
$$

When ignoring the spin, this means that (using the definition of $C_\eta(p)$):

$$
f^\dagger = K(p) c_{-p}
\tag{3.72}
$$

$$
K(p) = \frac{6}{|1 + e^{i\vec{p}_k\cdot\vec{\eta}}|^2 + |1 + e^{i\vec{p}_k\cdot\vec{\eta}^-}|^2 + |1 + e^{i\vec{p}_k\cdot\vec{\eta}^+}|^2}
\tag{3.73}
$$

Lastly, when in the very specific regime that equation 3.69 holds, it is possible to write down the quasi-particle spectral function $A(p,\omega) = Z(p)\delta(\omega - \varepsilon(p))$. In this case $Z(p)$ is given by equation 3.74.

$$
\begin{aligned}
Z(p) &= \left| \langle p | c_{-p} | 0^* \rangle \right|^2 \\
&= \left| \langle 0^* | f_p \frac{1}{K(p)} f^\dagger_p | 0* \rangle \right|^2 \\
&= \left| \frac{1}{K(p)} \right|^2 \\
&= \frac{1}{36} \sum_\eta |1 + e^{i\vec{p}\cdot\vec{\eta}}|^2 \\
&= \frac{2}{36} \sum_\eta \left(1 + \cos(\vec{p}\cdot\vec{\eta}) \right)
\end{aligned}
\tag{3.74}
$$

This would have been a very interesting result, would it not be the case that the regime in which this holds is mostly unknown. For the square case there is a very clear regime for which these particle can be treated as described above. But unfortunately there is no proper known regime for which this free Fermi gas-like description is valid. Especially since the restriction $p_1 = 0$ or $p_2 = 0$ leaves the system rather asymmetrical.

Chapter 4

Simulations of Fermionic Perturbations to the Triangular RK-Hamiltonian

In this chapter we will discuss the work done on finding the ground state energies for different versions of the two-dimer RK-Hamiltonian and a more general version of equation 3.6. These dimers are defined in chapter 3.

$$H = H_{RK} + t_{static} \sum | \diagup\diagup \rangle\langle \diagup\diagup | + t_{flip} \sum | \diagup\diagup \rangle\langle \diagup\diagup | + t_{rotation} \sum | \diagup\diagup \rangle\langle \diagdown |$$
(4.1)

Where, as before, the summations are over all triangular plaquettes, all orientations of these plaquettes ($\diagup\diagup$, $\diagup\diagup$, $\diagdown$ and $\diagdown$) and all possible rotations (so both clockwise and anticlockwise for the $t_{rotation}$-term. Note that 3.6 is a special case of equation 4.1.

The program used to calculate the ground state energies for this Hamiltonian starts out by creating all possible states for a given lattice (preferably $N \times N$) and then applying the Lanczos algorithm (see section 4.2.2) on a randomised and normalised begin state. For speed and control, C++ is used as the programming language.

4.1 Finding the State Space

The first thing to do is find an efficient way to find all states in the state space. For now the state space will consist of solely Bosonic dimers. The obvious choice for a complete (orthonormal) basis is to find all unique dimer coverings. An $N \times M$-lattice is created in the form of an array with one entry for each lattice site. Once a proper (no empty sites, no overlapping dimers) and unique dimer covering is found, it will be stored in a linked list for later use.

4.1.1 Failed Attempt: Brute Force Method

The first attempt of finding all coverings was made using a brute force approach. This approach gave each site a value between 0 and 3. The number 1 signified a horizontal dimer sprouting from it's site, 2 a vertical dimer and 3 was used as a diagonal dimer. Since a dimer always consists of a connection between two sites, the second site of each of these dimers would have the number 0. Which had the function of "recieving" of a dimer, initiated from a site with a 1, 2 or 3. An example of a covering with an array describing it can be found in figure 4.1. Keep in mind that what is called "vertical" is still not perpendicular to the horizontal direction in

physical reality. But since reality is reduced to a two-dimensional array, the term vertical refers to the vertical axis of said array.
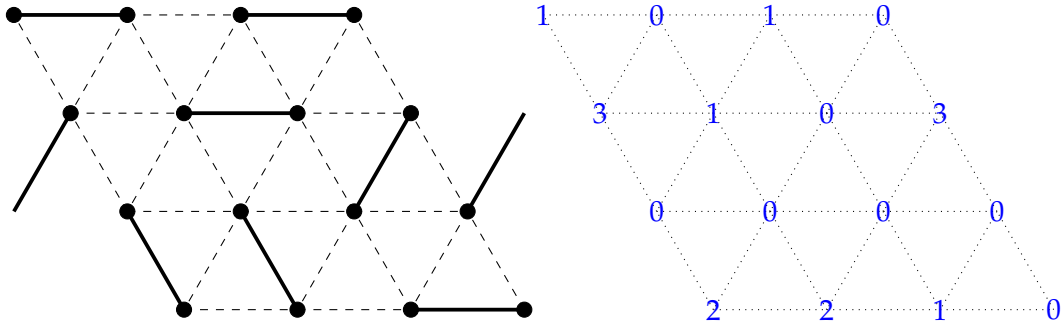

FIGURE 4.1: This figure shows an example covering (left) on a 4×4-lattice with dimers in all three possible orientations. On the right this same covering has been displayed as array with numbers corresponding to the dimer orientations as described above. Note that periodic boundary conditions are in place.

Once this notation has used, one can find all possible coverings by going through all possible $N \times M$ arrays filled with only the numbers 0 to 3. For each of these arrays the program needs to check whether it can be considered a proper covering. If this is the case, the covering will be copied and stored in the covering list before continuing to cycle through the rest of the potential coverings.

This method has one advantage: it is very easy to make sure one does not accidentally coverings twice. By taking one single cycle through all candidate coverings (from all zeroes to all threes) every proper covering is evaluated once. The major downside to this: an excessive amount of faulty coverings is evaluated before being dismissed. Since this brute force algorithm considers 4 numbers for each lattice sites, the time it takes to execute is proportional to $4^{N\times M}$. So in practice, this algorithm works fine for lattices with a size of up to about 4×4, and becomes outrageously slow for larger scales. To illustrate, running the program for a 4×4-lattice took about 20 seconds. By linear extrapolation (multiplication by 4^{36-16}) it was calculated to take over 600,000 years to go over all potential coverings for a 6×6-lattice.

4.1.2 Recursive Search

Since 600,000 years tends to be somewhat much for a master thesis a different approach was taken: iterative search. Rather than filling an entire array with numbers in hopes that it will be a well-defined covering, this method works by taking a partial covering (with part of not covered by dimers, yet) and trying to add a new dimer on the lowest empty site (the sites can be numbered any way, as long as it is consistent). For all the dimers that can be added to the lowest site, a new partial covering is obtained. The same process is applied to these new coverings, until it is a completely full covering or no more dimers can be added without overlapping each other. More detailed description follows later this section.

The way the dimers are represented by numbers has slightly changed, compared to section 4.1.1. Since this algorithm requires to be able to make dimers in all six directions there now are 6 directions, and the number 0 for empty sites. The numbers 1, 2 and 3 serve the same purpose as before (representing horizontal $(1,0)$, vertical $(0,1)$ and diagonal $(-1,-1)$ dimers respectively), but the "other end" of the dimer is no longer indicated by a 0. For the other end of a horizontal dimer a 4 is used,

making 4 represent a dimer in $(-1, 0)$-direction. The number 5 is the counterpart to the number 2, making the corresponding direction $(0, -1)$, and finally, 6 is the opposite of 1, namely: $(1, 1)$. See figure 4.2 to see the same covering as before being represented by this new notation.
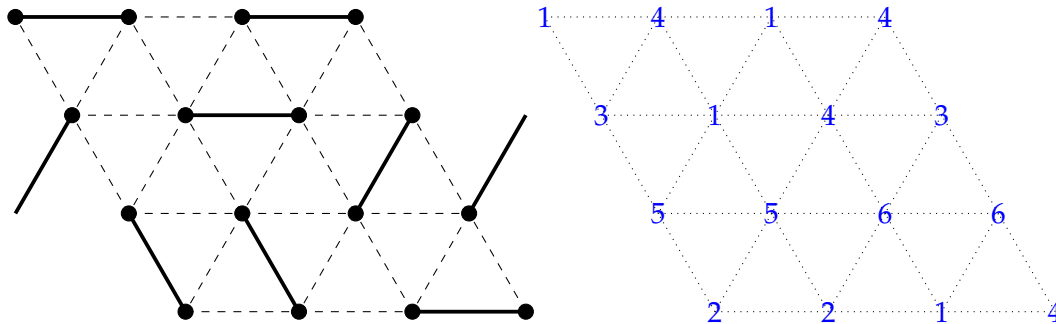

FIGURE 4.2: On the left side the same covering as in figure 4.1 is shown. On the right this covering is represented by the new notation: 1 is $(1, 0)$, 2 is $(0, 1)$, 3 is $(-1, -1)$, 4 is $(-1, 0)$, 5 is $(0, -1)$ and 6 is $(1, 1)$. The number 0 is not seen in this figure, as it represents an empty lattice site.

This new notation has four main advantages over the previous notation. In the first place, this allows for empty sites, which are crucial when working with partial coverings. The second advantage is that this makes running though 6 orientations less confusing when writing the code. Rather than running from 1 to 3 and then making 3 special cases for the zeroes, the program can simply run from 1 to 6. The third advantage is that this makes checking the lattice for flippable plaquettes, when building the Hamiltonian, a lot more straight forward. Not only for writing clear code, but also because less checks have to be done to reach a sound conclusion. The last advantage was accidental: because the way the program works (finding the lowest empty site and trying to add dimers from 1 to 6), all states are ordered. Ordered in the sense that if the numbers on each site (from low site number to high sit number) where written as digits of a number, representing the site, the list of these numbers would be ascending. This is useful for the Hamiltonian part of the program.

In figure 4.3 a piece of pseudo code is shown, to explain the process of finding all possible covering. This is a simplified version of the recursive function used in the actual program.

The search is initiated when an empty covering is given to the function called "RecursiveSearch" in figure 4.3. This can also be done with a non-empty (partial) covering, if all coverings with given fixed dimers need to be found. The initial partial or empty covering (called "PartialCovering") is given as an integer array with a length equal to the number of sites. Additionally a second integer array of the same size is created, named "NewPartialCovering", and an integer is created to saved the lowest empty site number (called "LowestEmptySite" in the figure). Next up is a for-loop, looping through the number 1 to 6, for the six possible dimer orientations. For each of those, copy the initial covering (PartialCovering) to NewPartialCovering. Then see if the given orientation can be added with the function AddDimerPossible. If not: try the next orientation until it works, or turns out to be impossible. If it works, add the new dimer to NewPartialCovering. Then check whether the covering is complete with "NoEmptySites", and save if it to the list if it is. If NewPartialCovering still has empty sites, call in a new instance of the function RecursiveSearch to

add more dimers. Once a complete dimer covering has been found, the current instance closes to go back one layer and try the rest of the options, to eventually find all possibilities.

```
void RecursiveSearch(int PartialCovering [NumberOfSites]){

    int NewPartialCovering [NumberOfSites];
    int LowestEmptySite = FindLowestEmpty(PartialCovering);

    for(int i = 1; i <= 6; i++){     // i is dimer direction
        NewPartialCovering = PartialCovering;  // make a copy
        AddDimerPossible(PartialCovering,LowestEmptySite,i);

        if(AddDimerPossible){
            AddDimer(NewPartialCovering,LowestEmptySite,i);

            if(NoEmptySites(NewPartialCovering)){
                SaveToList(NewPartialCovering);
            } // if(NoEmptySites)
            else{ // starts following iteration
                RecursiveSearch(NewPartialCovering);
            } // else

        } // if(AddDimerPossible)
    } // for i
} // void RecursiveSearch
```

FIGURE 4.3: This figure shows a sketch of the recursive function used
in the search algorithm.

A helpful detail considering this approach, is that there are no prerequisites for the initial partial covering (other than having an even number of empty sites). So by inserting a partial covering consisting of a single Fermionic dimer (which can be indicated by new number), one can find all coverings for fixed doping, making the step from all undoped to all doped coverings very small.

This approach is significantly faster than the aforementioned brute force approach. Since each dimer covers two sites, going from empty to full on an $N \times M$-lattice takes $\frac{N \times M}{2}$ steps with 6 directions each. But this number can be reduced, since for the first, since only the very first site truly can be pointed in all six directions. The next $N - 2$ (assuming N to be the horizontal direction, here) only have five options or less. This because a number of neighbouring sites is already occupied. The Nth site only has four possibilities, since both the previous and very first site are both filled and nearest neighbours. Then for each site on a new row there are only four options too, except the last one, for which there are only two. The last site on a row has only two options as well and the very last site of the very last row has now choice, whatsoever. Every other site, has three options to choose from. All together, this reduces the number of attempt to scale with: $6 \cdot 5^{N-2} \cdot 4^{M-1} \cdot 2^{M-1} \cdot 3^{\left(\frac{N \times M}{2} - N - 2M + 4 - 1\right)} = \frac{81}{100} \cdot \left(\frac{5}{3}\right)^N \cdot \left(\frac{8}{9}\right)^M \cdot 3^{\frac{N \times M}{2}}$. Or for an $N \times N$-lattice:

$$t_{computation} \propto \frac{81}{100} \cdot \left(\frac{40}{27}\right)^N \cdot 3^{\frac{N^2}{2}} \tag{4.2}$$

Which is drastically faster than the 4^{N^2} from the brute force approach. A 6×6 lattice can be filled in about 12 seconds, using this algorithm.

4.1.3 Early Results

This section gives a brief discussion considering the results from generating the state spaces for $N \times N$-lattices using the recursive algorithm described above.

	$N_{coverings}$	$t_{computation}$	$N_{staggered}$
2×2	12	∼ 0 sec	0
4×4	1 920	0.003 sec	12
6×6	10 045 824	13 sec	0

FIGURE 4.4: The simple statistics considering the generation of the state space for all feasible $N \times N$-lattices. Result of the recursive search method described in section 4.1.2.

Figure 4.4 shows the basic results after running for all possible $N \times N$-lattices. Lattices with odd N are excluded, since an even number of sites is needed for dimers to completely cover it. Lattices with even $N > 6$ are not possible to calculate for time's sake: extrapolating from the computation time ($t_{computation}$) for the 6×6-lattice with equation 4.2 gives a run time of over 4 years for the 8×8-lattice. Since the computation times differ from computer to computer, calculating all coverings for the 8×8-lattice within a more reasonable time seems plausible, just not necessary considering the time it would take.

When looking at the number of unique coverings ($N_{coverings}$) grows drastically with the lattice size. Because of this, only the output of the 2×2-lattice included (in figure 4.5) in this thesis. Keep in mind that when translating the numbers to coverings, one should read from left to right and from low to high. As an example, the covering in figure 4.2 has the number 2214...1414 (and not 1414...2214). Reading these number differently does not change the physics, as long as it is applied consistently.

1414	1441	2255	2552
3366	3636	4114	4141
5225	5522	6363	6633

FIGURE 4.5: This figure shows the output dimer coverings of the recursive algorithm for a 2×2-lattice in the form of a single 4 digit number.

When looking at the figure, one sees that the list of covering in the previous figure is ordered from small to large. This is a very useful (though originally unintentional) feature of the recursive algorithm. But by starting at the lowest site with the lowest orientation number, and working to higher sites and orientation numbers, the coverings are ordered from low to high by construction. The reason this is useful, is that when looking up a state (for the Hamiltonian function, described in section 4.2), the ordering can be used to skip large parts of the coverings.

One last detail about figure 4.4 worth considering is the amount of staggered states for $2N \times 2N$-lattices. Only the 4×4 has a non-zero amount of staggered states.

The 2×2-lattice is simply too small for that, since every possible covering has exactly 2 flippable plaquettes. The 4×4 staggered state in figure 1.11 (on the right) can be used as a basis cell for staggered states on $2N \times 2N$ (with N even). By repeating this basis one can generate staggered states for lattices with said even N. This still leaves the question whether staggered states exist for $2N \times 2N$ with odd N. The data from the aforementioned table shows that there are none for the 6×6-lattice, suggesting that this these do not exist. Although unnecessary for the simulations done for this thesis, this can be an interesting detail to look further into.

4.2 Computations on the State Space of Dimer Coverings

Now that all dimer coverings are generated (with or without doping), the program needs to be able to calculate the ground state energy of the Hamiltonian (equation 4.1). To do so, a way to store a current state is needed, along with a way to calculate the working of the Hamiltonian on this state (similar to the work done before on the square lattice[1]). Since this program works in the (orthonormal) basis of all unique dimer coverings on a given $N \times M$-lattice, the obvious choice is to attach a complex number (or two real floating point numbers) to each covering, turning the list of coverings into a vector. In practice it will be turned into three vectors: one current vector (v_{curr}), one previous vector (v_{prev}, not more than one previous state will be needed) and one new state (v_{next}, because the Hamiltonian must be able to work on a state without losing the data of the original).

The undoped part of the Hamiltonian is implemented in a very straightforward way. The function goes over all coverings in search of flippable plaquettes. For each dimer there are 4 potiental plaquette flips. Since there are 3 dimer orientations is enough to describe all possible dimers, this results in 12 potential 12 plaquettes per dimer, or six per site. The program used to generate the data for this thesis checks three plaquettes per site and checks for both possible flips (those two flips are each other's inverse). For each flipable plaquette found on covering C, a temporary copy (called D) of the covering is made, on which the flip will be applied. Then the list of coverings is searched (using its ordering to speed it up) and when covering D is found, the value of the component corresponding to D and C of v_{next} (called $v_{next,D}$ and $v_{next,C}$, respectively) will be changed as follows:

$$\Delta v_{next,C} = v \cdot v_{curr,C} \tag{4.3}$$
$$\Delta v_{next,D} = -t \cdot v_{curr,C} \tag{4.4}$$

In which v and t are the parameters of H_{RK} (see equation 1.25). Once every covering has been gone through this process, the vector $v_{next} = Hv_{curr}$.

When turning the system into a doped system the only thing that needs to be done is to add perturbation in the form of one or more Fermionic dimers. To prevent the Hilbert space from drastically increasing in size, this method will be constrained to perturbations of a single Fermionic dimer. So the state space that needs to be found would on first glance be a lot larger than the undoped state space. This state space can be found by placing a single Fermionic dimer on an empty lattice and then filling the rest the lattice with with Bosonic covers in all configurations possible, using the recursive algorithm from section 4.1.2. This then has to be done for each possible position of the Fermionic dimer, requiring the recursive algorithm

---

[1]Punk, Allais, and Sachdev, 2015

the be applied $3N \times M$ times. Luckily there are a two ways to reduce the amount of states needed for calculations. The first one, which can also be applied to the undoped case, is to restrict the Hilbert space to a single topological sector, as described in section 1.2.4. The topological sector used during this thesis was defined by the amount of dimer crossings through the red an blue lines in figure 4.6. Keep in mind that Fermionic and Bosonic dimers are interchangeable for the purpose of finding the topological sector. The topological sector used for all calculations, later on, is (*even*, *even*).
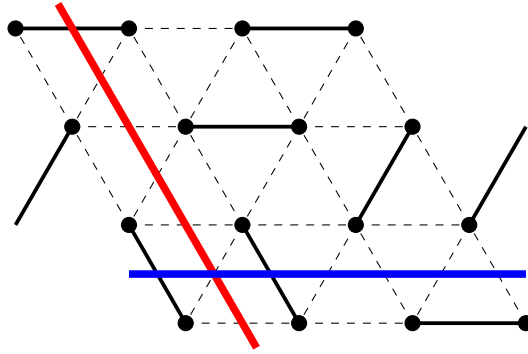

FIGURE 4.6: This figure shows which paths where chosen to determine the topological sector of which the covering was part. In this example the covering is part of sector (*odd*, *even*).

4.2.1 Periodic and Twisted Boundary Bonditions

The next principle used to reduce the state space is by using the periodic boundary conditions. Many of the generated states are in essence different states with a spatial translation. Using periodic boundary conditions one can relate these by multiplication with a phase factor. If $|C\rangle$ is a given base state and $|C'\rangle$ is the same state, but translated by a $\vec{x}_{trans}$. Those state then are related as shown in equation 4.5, see figure 4.7 for an example with $\vec{x}_{trans} = a\hat{x}$.

$$|C\rangle = e^{-i\vec{p}\cdot\vec{x}_{trans}}|C'\rangle \tag{4.5}$$

Where $\vec{p}$ is the momentum of the state. The sign of the phase factor can be both negative and positive, but this convention has been chosen for the simulations in this thesis. By equation 4.5 the state space can be drastically reduced by simply translating the Fermionic dimer to the origin (and the rest of the covering along with it). When this is done the amount of timed the recursive algorithm has to be applied can be reduced from $3N \times M$ to 3. Instead one has to keep the phase factors in account, but luckily this adds momentum to the system in a natural way. So not only can the ground state be found, the ground state can be found as a function of momentum.

After applying the periodic boundary conditions, information about momentum can be obtained. The momentum states possible in a finite lattice are limited to $N \times M$ values, being $\vec{p} = \frac{n}{N}\vec{p}_x + \frac{m}{M}\vec{p}_y$ with $n = 0, 1, ..., N-1$ and $m = 0, 1, ..., M-1$. With $\vec{p}_x$ and $\vec{p}_y$ the reciprocal lattice vectors. For the triangular case the reciprocal lattice vectors are $\vec{p}_x = \frac{2\pi}{a}\hat{x} + \frac{4\pi}{\sqrt{3}a}\hat{y}$ and $\vec{p}_y = \frac{4\pi}{\sqrt{3}a}\hat{y}$, with $\vec{r}_x = a\hat{x}$ and $\vec{r}_y = -\frac{1}{2}a\hat{x} + \frac{\sqrt{3}}{2}a\hat{y}$ the (non-reciprocal) lattice vectors. The symbol a is the distance between neighbouring
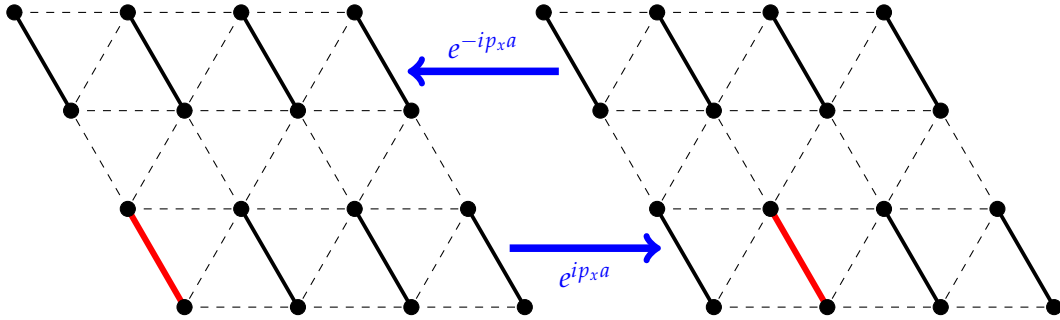
FIGURE 4.7: This figure shows two doped coverings that are different by only a spatial translation. The Fermionic dimer is coloured red. The two coverings are related as follows: $|C_{left}\rangle = e^{-ip_x a}|C_{right}\rangle$, where a is the distance between neighbouring sites.

lattice sites. By the definition of the the (reciprocal) lattice vectors, the phase factor $e^{-i(n'\vec{r}_x + m'\vec{r}_y)\cdot\vec{p}} = e^{-i(\frac{n'n}{N} + \frac{m'm}{M})2\pi}$, which makes the computation simpler.

It is possible to expand on the periodic boundary conditions to allow for more momentum values using a trick called twisted boundary conditions. Other than restricting oneself to the aforementioned allowed phase factors, one chooses an arbitrary phase to allow for a higher resolution in momentum. These momentum values then still lay in the first Brillouin zone, off course. This artificial increase of resolution in momentum is the same as pretending the lattice is larger than it actually is. All finite size effects of the actual lattice will remain in place. So the state space stays smaller than what would otherwise be the case for a larger lattice. Additionally, this means that the effect of one fixed dimer (the Fermionic one, for example) has more impact on the rest of the dimers than usual. Lastly, the doping does not translate over well to larger lattices. For a small lattice, a doping of one dimer is larger (relative to the total amount of particles) than it would be for a bigger lattice. These effects are usually worse for systems with a long correlation length, but since dimers on a triangular lattice are described by a Z_2 spin liquid[2], they generally have a short correlation length. The expectation is that the effects will acceptable when applied to a 2*x*2-lattice. This will be empirically tested in section 4.3.1.

4.2.2 Lanczos Algorithm

From the previous sections it is now clear how the state space is created and how the Hamiltonian naturally includes momentum into the picture. But just knowing how to apply the Hamiltonian does not lead to the ground state, yet. To go from an arbitrary state to the ground state an algorithm will be used, called the Lanczos algorithm (not to be confused with the Lanczos block algorithm or Lanczos resampling). This is a fairly well-known algorithm used to find the eigenvalues of Hermitian $n \times n$ matrices. In this case this matrix is the Hamiltonian (with n the number of states in the state space). Every iteration of the algorithm finds one new eigenvalue of the matrix, eventually finding them all (after n steps).

This algorithm uses the fact that there is always a highest eigenvalue in a finite state space. A simplified version of the algorithm takes both the Hamiltonian and beside that real number larger than the highest eigenvalue: λ_+. Then a random normalised vector (v_0) is chosen to begin with. The simplified algorithm is shown in equations 4.6 to 4.8.

---

[2]Moessner and Raman, 2008

$$v_i' = (\lambda_+ - H)v_{i_1} \tag{4.6}$$

$$v_i = \frac{v_i'}{|v_i'|} \tag{4.7}$$

$$\lambda_i = \langle v_i, H v_i \rangle \tag{4.8}$$

The v_i are the normalised versions of v_i', and λ_i is the energy of v_i. Since λ_+ is larger then any eigenvalue of H, $\langle v_{eigen}, (\lambda_+ - H)v_{eigen} \rangle$ will always be larger than 0, with the lowest eigenvalue giving the largest contribution. When this algorithm is repeated, the prefactor of each eigenvector will be $(\lambda_+ - \lambda_{eigen})^n$ after n steps. This factor will grow the fastest for the lowest eigenvalue (the ground-state-eigenvalue), so eventually all other contributions will be negligible. After enough (no upper limit) iterations v_i wil be the ground state: $\lim_{i \to \infty} v_i = v_{ground}$ and $\lim_{i \to \infty} \lambda_i = \lambda_{ground}$. This simplified version of the algorithm works, but is rather slow. When this was tested on a 2×2-lattice for Rokhsar-Kivelson Hamiltonian along the RK-line, with a known ground state energy of 0. This algorithm took around 350 iterations to be at a precision of 10^{-5}.

The (actual not-simplified) Lanczos algorithm is a lot faster than the simplified version, though a bit more complex. This algorithm, too, begins with an arbitrary normalised ground state v_0, and going to v_1 works the same. From there the algorithm deviates from the previous version by following the steps shown in equations 4.9 to 4.12.

$$\alpha_i = \langle v_i, H v_i \rangle \tag{4.9}$$
$$v_{i+1}' = (H - \alpha_i)v_i - \beta_{i-1}v_{i-1} \tag{4.10}$$
$$\beta_{i+1} = |v_{i+1}'| \tag{4.11}$$

$$v_i = \frac{v_i'}{|v_i'|} \tag{4.12}$$

Keep in mind that if one chooses $\beta_0 = 0$, the first step is reduced to the simplified case from equation 4.6 to 4.8. Keep in mind that both this algorithm and the previous version assume that $v_i' \neq 0$. When applying the algorithm, this is practically always true, so if this would happen, the program would give an error. One can continue by choosing (if $v_i' = 0$) a new arbitrary normalised vector for v_i, which is orthogonal to all v_j with $j < i$. This last part was not necessary to implement since the probability of this happening is near zero.

$$T = \begin{pmatrix} \alpha_0 & \beta_1 & & & & 0 \\ \beta_1 & \alpha_1 & \beta_2 & & & \\ & \beta_2 & \alpha_2 & \ddots & & \\ & & \ddots & \ddots & \beta_{n-2} & \\ & & & \beta_{n-2} & \alpha_{n-2} & \beta_{n-1} \\ 0 & & & & \beta_{n-1} & \alpha_{n-1} \end{pmatrix} \tag{4.13}$$

The energy of the vectors v_i obtained in by executing the Lanczos algorithm is equal to the value β_i. Unlike the previous algorithm this value is not the parameter that will slowly converge to the ground state. To find the ground state, all found values α_i and β_i are needed in the form of a tridiagonal matrix T, as seen in equation 4.13. This

is the Matrix after n iterations. Keep in mind that other sources might start at $i = 1$, rather than $i = 0$ The tridiagonal matrix works on the vector space consisting of the span of v_i, which is $n + 1$-dimensional. The $n + 1$ eigenvectors and eigenvalues of T are eigenvectors and -values of H as well. So solving the eigenvalue problem for T gives $n + 1$ of which the lowest can be selected. This algorithm strictly guarantees that for a D-dimensional Hamiltonian in D steps (giving values $0, 1, ...D - 1$ for i) all eigenvalues can be found. Finding the ground state energy (lowest eigenvalue) is in practice a lot faster. Choosing the lowest eigenvalue quickly converges to the real ground state eigenvalue. For the RK-line, with an exact ground state energy of 0, the algorithm takes about 100 iterations to reach a precision 10^{-15}, which is less than the numerical precision of the program itself.

4.3 Results

The first few tests were done on the undoped dimer model around the RK-point, mostly to act as a control experiment. At the RK-point and at $v > |t|$ the systems quickly converge to zero ground state energy, as expected. At values where $0 < v < |t|$ the energy was negative, more so when v got smaller, and as a last test for $v < -|t|$, the the ground state energy went to $\frac{1}{2}Nv$. Hence, the program quickly passed the undoped test.
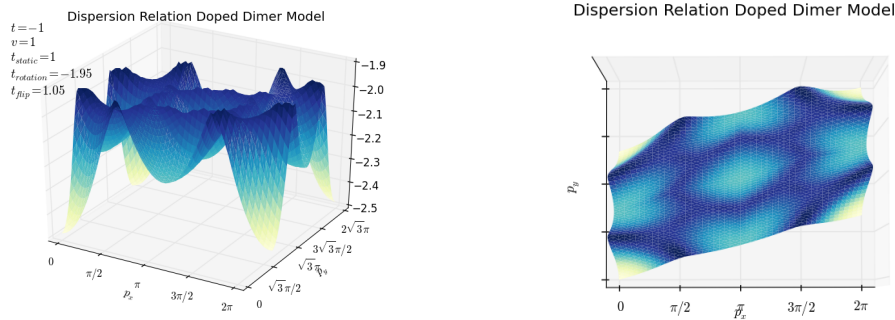
FIGURE 4.8: This figure shows the Fermionic dispersion of a 4×4-lattice with a resolution of 12 and Hamiltonian parameters similar to those used in Punk, Allais, and Sachdev, 2015. Both figures show the same data from a different angle.

The interesting results begin when the doping is turned on (one single Fermionic dimer on the lattice) and the twisted boundaries are applied. Before going there it is important to set some standards for all results from here on, unless explicitly specified otherwise. First: all data, except part section 4.3.1, is generated using a 4×4-lattice and twisted boundary conditions. The "resolution" of an image, is the multiplier for the that determines the effective lattice size after applying twisted boundary. To be completely explicit: if a figure is made using resolution R, the amount of sites on the effective lattice will be $4R \times 4R$. The figure will consist of $(4R + 1) \times (4R + 1)$ data points, since the boundary is included on all sides. The values for momentum are always given to be between null and 2π, as if the lattice has size 1 (not the lattice constant, the size of the entire lattice). All data points are

calculated up to 100 lanczos iteration, or to the point where a new Lanczos iteration makes a difference in energy of less than 10^{-9} (less than numerical precision for the output). In figure 4.8 an example is given with a resolution of 12, making it an effective 48×48-lattice.

4.3.1 Estimating the Effects of Twisted Boundary Conditions

It may not come as a surprise that using a high resolution comes at the cost of losing precision. This because the original lattice and state space will be significantly smaller than the lattice that is being imitated. To give an estimate of the discrepancy between the actual lattice and the twisted boundary version, figure 4.9 shows the comparison between an actual 6×6-lattice and a 6×6-lattice imitated by a 4×4-lattice with twisted boundaries.
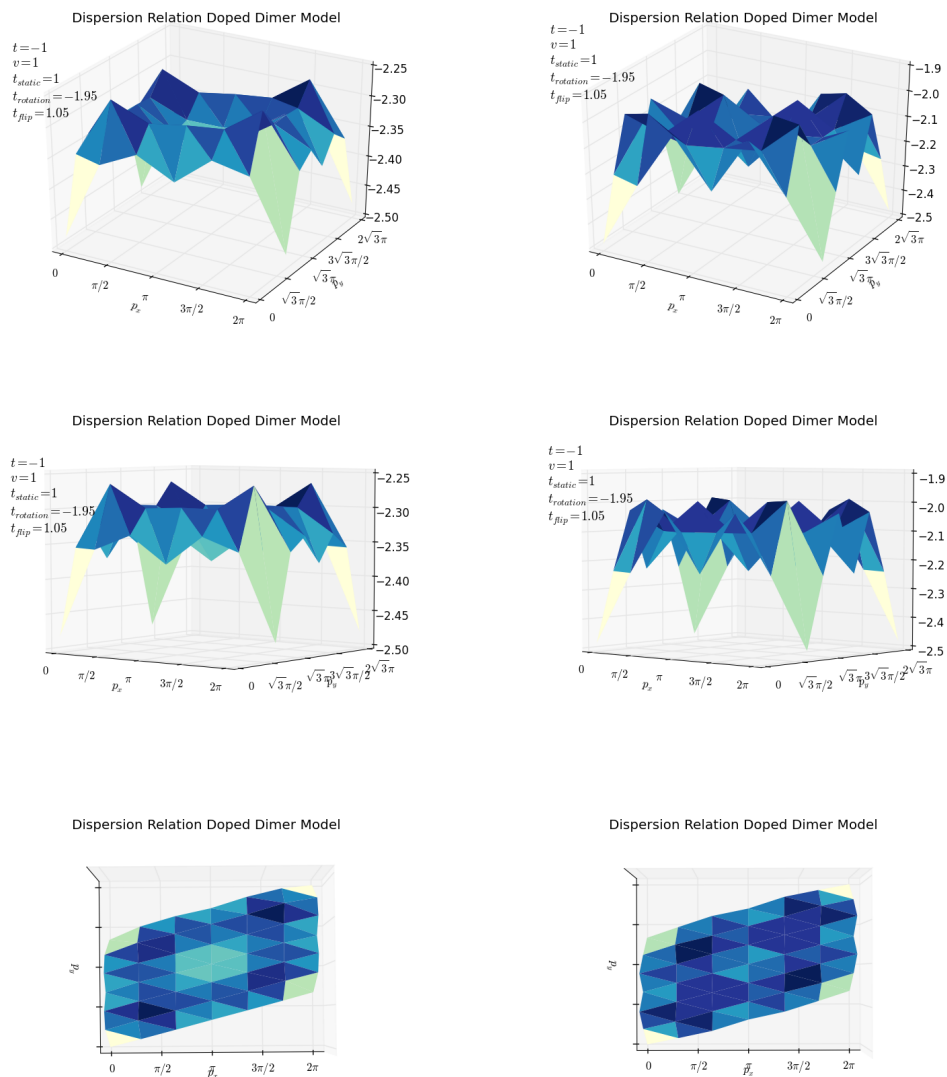
FIGURE 4.9: This figure shows both a real 6×6-lattice (left) and a 4×4-lattice (right) twisted to have the effective size of a 6×6-lattice. The data is shown under different angles for better comparison.

Comparing the 6×6 lattice with the twisted 4×4 lattice from a visual standpoint shows quite some similarity. The corners, $(n2\pi, m2\pi)$ with n and m integer, are the lowest point in both cases with a value of approximately -2.5. From the corner to the middle, the energy quickly increases to around -2.25 for the 6×6-lattice and around -1.9 for the twisted 2×2-lattice. Then, further to the middle the value goes down to roughly -2.35 and -2.2, respectively. The dale in the middle is more expressed in the 6×6-lattice, but it is observable in both cases. Because of low resolution it is hard to say whether the ring around the middle that is clearly visible in the higher resolution version of the 4×4-lattice (figure 4.8) is present on the 6×6-lattice, though it does not seem that way. A way to quantify the difference between the real 6×6-lattice and the twisted 4×4-lattice, is to plot their ration for each point on momentum space in a graph, as done in figure 4.10.
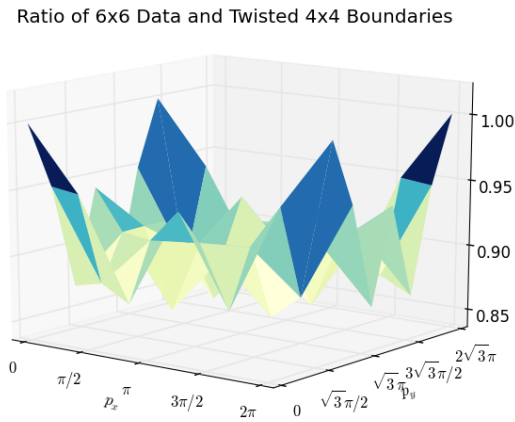
FIGURE 4.10: This figure shows the the ratio of the dispersion relation for the 6×6-lattice and the twisted 4×4-lattice as a function of momentum $(E_{6\times6}(p)/E_{twisted}(p))$.

Apart from the corners, where the ratio $E_{6\times6}(p)/E_{twisted}(p)$ seems to be 1, the value of $E_{6\times6}(p)/E_{twisted}(p)$ seems to vary between 0.95 and 0.85. So a deviation of roughly 10% seems to be correct, for the twisted lattice. This difference will likely get larger when the resolution increases, though the obtaining numerical evidence for this would take outrageously long.

Even though an error of 10% is rather large, the twisted 4×4-lattice is still the optimal lattice to use for calculations. The reason for this, is that the data for the twisted 4×4-lattice took less then 9 seconds to generate and the data for the 6×6-lattice was generated over the course of 3 days (on a faster computer, evident from executing the same programs om both). Because the amount of time save is so massive, and the generated error by using the twisted boundaries was only 10%, it is still worthwhile to do analysis using the twisted boundaries, as long as the numbers are not taken too precisely.

There is one additional difference between the $4\times$- and 6×6-lattice other than the scale. As shown in section 4.1.3, there are no staggered states on a 6×6-lattice, while there always are staggered states on $2n \times 2n$-lattices with even n. Because of this, taking a lattice without staggered states may potentially increase the error when trying to twist a lattice with staggered states into it.

4.3.2 Deviating from the RK-Line

The most obvious place to start looking at dispersion relations, is near the RK-line. On the RK-line everything is zero, and small deviations near the near the line are easy to predict. To begin, look at figure 4.11.
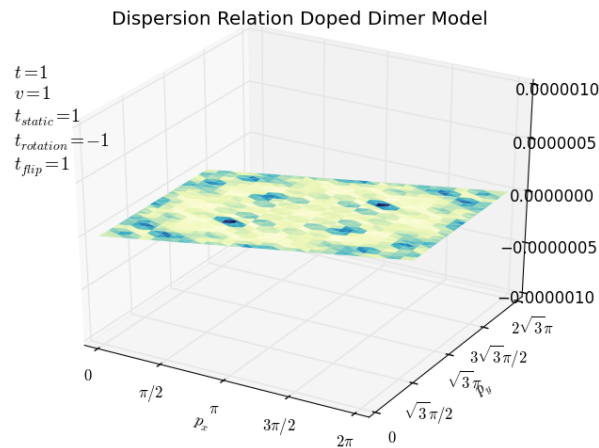

FIGURE 4.11: This figure shows the dispersion relation at the Fermionic RK-line, with a resolution of 6.

Figure 4.11 shows the very flat dispersion relation on the RK-line. Do not get confused, the difference in colour is smaller than 10^{-8}, all deviation from naught is only due to the fact that not every point converges at the exact same speed. If patterns seem periodic, this is due to the fact that they are, and this fact is used. So the relatively dark blue points around the centre are the same deviation, repeated multiple times. The symmetry of the system has been used to avoid calculating points, that are guaranteed to be the same, twice. All other versions of the RK-line (with $t = -1$, $t_{rotation} = 1$ or both) give the same result, with deviations smaller than 10^{-8}.
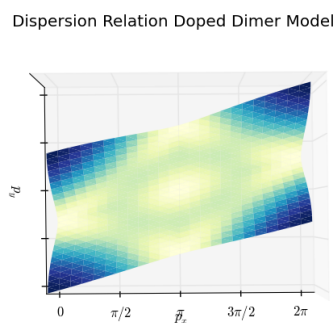
FIGURE 4.12: This figure shows the top view of the dispersion relations shown in figure 4.13, for $\delta_u < 0.06$.

Adding a perturbations to the RK-line can be done as described in section 3.2.1. Which in this case means adding a value δ_u to t_{flip}, making $t_{flip} = 1 + \delta_u$, since other deviations are no dimer swaps. According to equation 3.50 and 3.55 the resulting energy $\varepsilon(p)$ should scale linearly with δ_u. Figure 4.13 shows four different dispersion relations, from $\delta_u = 0.0001$ to $\delta_u = 0.1$ in powers of ten. The figures for $\delta_u = 0.01$ and smaller look identical, up to scale, yet the figure where $\delta_u = 0.1$ shows a "dent". Repeating this for different values of δ_u indicates that the transition happens between $\delta_u = 0.062$ and $\delta_u = 0.065$, which gives an upper bound for δ_u above the first order perturbation theory done in section 3.2.1 does no longer hold. Being more precise about this is not useful, since there will be a difference due to the twisted boundaries anyways.
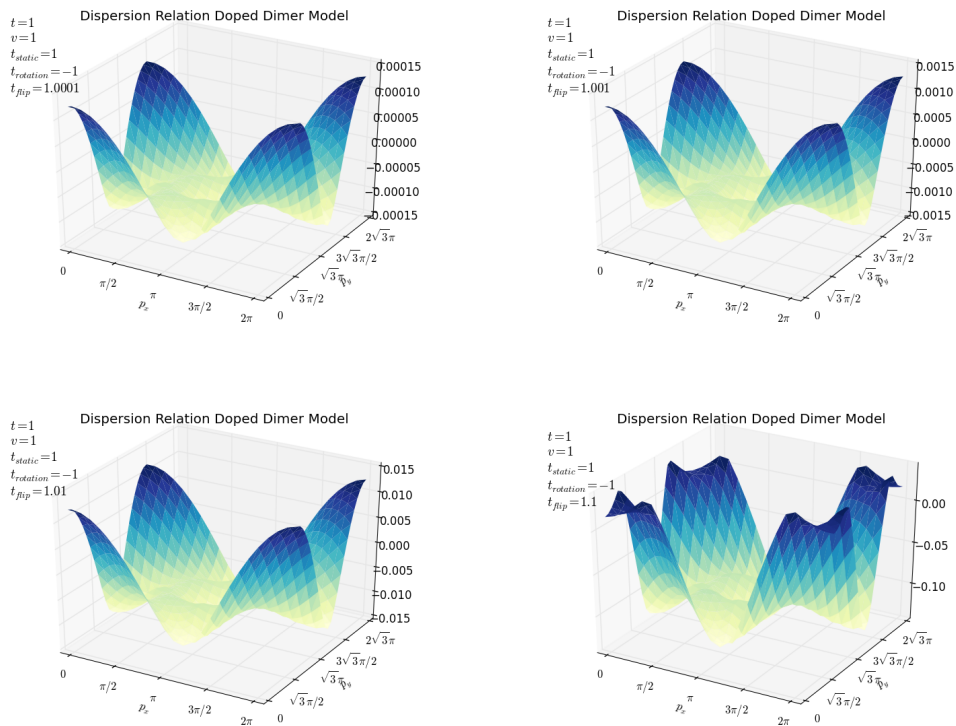
FIGURE 4.13: This figure shows dispersion relations for different values of δ_u at a resolution of 6. The top view for the first three is shown in figure 4.12.

The results in figure 4.13 are all done with positive perturbations, letting δ_u be negative gives the results shown in figure 4.14. The shape of the results is the same as for $0 < \delta_u < 0.06$, but with the opposite sign (as it should be). When δ_u starts getting bigger (more negative) it starts deviating from this shape. This is clearly visible in for $\delta_u = -0.25$, though is subtly showing for $\delta_u = 0.1$ as well. When trying to find the values for which the assumption holds, it seemed that around $\delta_u = -0.06$ it started to deviate. So the first order perturbations theory seems to hold for roughly $-0.06 < \delta_u < 0.06$.

When instead perturbing $t_{rotation}$, rather than t_{flip}, the results seems to look similar in shape to the previously discussed results. See figure 4.15 for an example with $t_{rotation} = -1 + \delta_u$, for $\delta_u = \pm 0.01$. Even though the shape of the graphs is similar, there is one main difference. For positive (or negative) δ_u, the entire dispersion relation is above (or below) zero, though for perturbations in t_{flip}, this was around zero
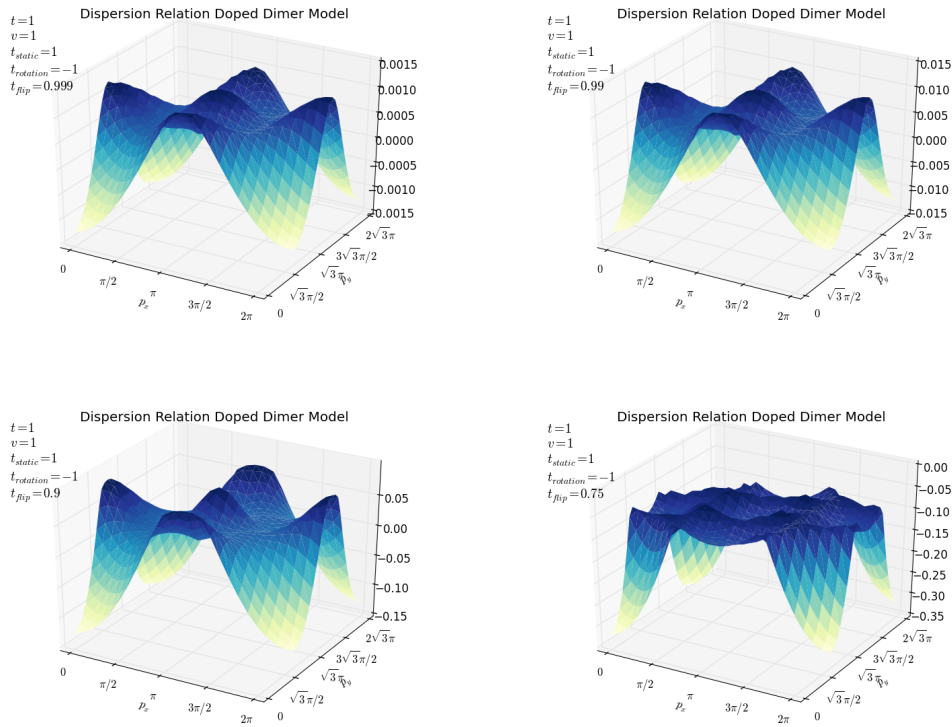
FIGURE 4.14: This figure shows dispersion relations for different values of δ_u at a resolution of 6.

(half above, half below). This suggests that even though this energy is not given by equation 3.50, it very well may be similar in form.

The exploration of the first order perturbations are by no means conclusive evidence about the correctness of equations 3.50 and 3.55. It does, however indicate that the ground state of the extended RK-line is somewhat stable when it comes to deviations. Since this ground state energy is nil, all perturbations in first order $\delta_u H'$ will give an energy proportional to δ_u, as long as the first order approximation holds. Which is equivalent to saying that the ground state does not change. Hence, the ground state is stable for small perturbations. To definitively prove that

4.3.3 Further Discussion

Something that is hard to see on the figures in section 4.3.1 and 4.3.2 is the hexagonal structure of the first Brillouin zone. This is mostly because the shape in which the data is presented is a slightly deformed parallelogram. This is done to present the data in a clearer way, but the downside is that the horizontal and vertical axes are no longer scaled one-to-one. To show the hexagonal structure of the dispersion relation of one of the previous images (where $t_{flip} = 1.01$), figure 4.16 is made. It shows a hexagonal structure, with the origin as its centre, by using the periodicity of the dispersion.

To prove that the dispersion has a hexagonal structure, note that the maxima of the dispersion are at the corners of the parallelogram (in all previous dispersions). The first corner is located on the origin, while the second is located along the y-axis, at a distance of $\frac{4}{\sqrt{3}}\pi$. The third is located at $(2\pi, \frac{2}{\sqrt{3}}\pi)$, which is a distance of $\frac{4}{\sqrt{3}}\pi$ away from the first two corners. So these three points form an equilateral triangle.
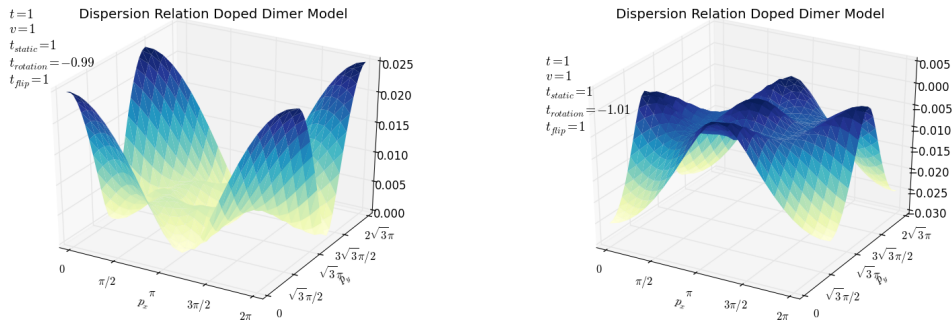
FIGURE 4.15: This figure shows dispersion relations for the perturbations $t_{rotation} = 1 + 0.01$ (left) and $t_{rotation} = 1 - 0.01$ (right) at a resolution of 6.
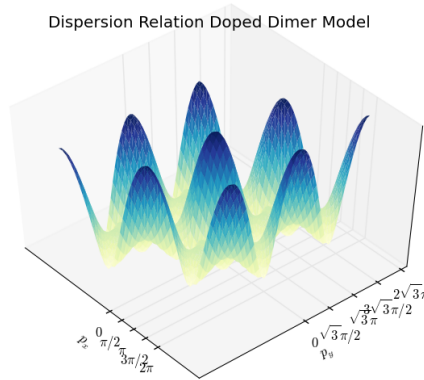

FIGURE 4.16: This figure shows the hexagonal structure of the dispersion relation, by showing the four Brillouin zones around the origin. The resolution of this image is 6.

The last maximum lies a distance of $\frac{4}{\sqrt{3}}\pi$ above the third, at $(2\pi, \frac{2}{\sqrt{3}}\pi)$, which lies at the same distance away from the second point, forming another equilateral triangle.

By now it is clear that the code written for this thesis is capable of producing dispersion relations. Beside the obvious value of this, namely: finding said dispersion relations, these results can be used to find the size of the Fermi surface. This is simply done by setting the chemical potential to a given value, and finding the contour of where the dispersion is equal to this chemical potential. The reason that this is valuable is that this is something that can be measured with the photo-emission spectrum. This creates a way to experimentally verify the validity of the numerical predictions made in this thesis.

Chapter 5

Conclusions and Outlook

In chapter 2 of this thesis, an exact expression is found for the classical two-variable, or single-dimer, correlations on the triangular lattice. Using Wick's theorem they can be used to find any more-dimer correlation. This expression can be, and is, numerically evaluated to find that the classical dimer-dimer correlations decay exponentially. Which is consistent with earlier predictions[1].

Chapter 3 introduces a Fermionic dimer to the system introduced in chapter 1. Because of this, the triangular RK-Hamiltonian is expanded and, along the extended RK-line, the exact ground state is found (for large lattices). This system can be analytically perturbed to find that each Fermionic adds a new energy term. Unlike the square lattice, however, it is not possible to find critera for which the system can be seen as a Fermi liquid of quasi-particle excitations.

In chapter 4 a program is described that finds the ground state for a given triangular Hamiltonian. This is then used to explore the perturbed and unperturbed Hamiltonians described in chapter 3. The program shows a lot of potential and seems to work very well, both on and around the RK-lineTo properly show whether the analytical predictions made are correct or not, one could use a program like Mathematica to compare the exact expression for $\varepsilon(p)$ with the numerical results. In addition to this, taking a contour of the dispersion at a given height allows for experimental verification of the theory.

---

[1]CHECK

Bibliography

Anderson, P. W. (1987). "The Resonating Valence Bond State in La2CuO4 and Superconductivity". In: *Science* 235 (4793), pp. 1196–1198. DOI: 10.1126/science.235.4793.1196. URL: http://science.sciencemag.org/content/235/4793/1196.

Badoux S., Tabis W. Laliberté F. Grissonnanche G. Vignolle B. Vignolles D. Béard J. Bonn D. A. Hardy W. N. Liang R. Doiron-Leyraud N. Taillefer Louis Proust Cyril (2016). "Change of Carrier Density at the Pseudogap Critical Point of a Cuprate Superconductor". In: *Nature* 531, pp. 210–214. DOI: 10.1038/nature16983. URL: https://doi.org/10.1038/nature16983.

Feldmeier, J. (2018). "Master's Thesis Spectral Functions and Exact Solutions in a Quantum Dimer Model for Pseudogap Metals". MA thesis. Ludwig-Maximilians-Universität.

Feldmeier, Johannes, Sebastian Huber, and Matthias Punk (2018). "Exact Solution of a Two-Species Quantum Dimer Model for Pseudogap Metals". In: *Phys. Rev. Lett.* 120 (18), p. 187001. DOI: 10.1103/PhysRevLett.120.187001. URL: https://link.aps.org/doi/10.1103/PhysRevLett.120.187001.

Fendley, P., R. Moessner, and S. L. Sondhi (2002). "Classical dimers on the triangular lattice". In: *Physical Review B - Condensed Matter and Materials Physics*. ISSN: 1550235X. DOI: 10.1103/PhysRevB.66.214513. arXiv: 0206159 [cond-mat].

Fradkin, E. and S Kivelson (1990). "Short Range Resonating Valence Bond Theories and Superconductivity". In: *Mod. Phys. Lett. B* 4 (3), pp. 224–323. DOI: 10.1142/S0217984990000295. URL: https://www.worldscientific.com/doi/abs/10.1142/S0217984990000295.

Kasteleyn, P.W. (1961). "The statistics of dimers on a lattice". In: *Physica*. ISSN: 00318914. DOI: 10.1016/0031-8914(61)90063-5. arXiv: 0901.2686.

Kohmoto, M. and Y. Shapir (1988). "Antiferromagnetic correlations of the resonating-valence-bond state". In: *Phys. Rev. B* 37 (16), pp. 9439–9442. DOI: 10.1103/PhysRevB.37.9439. URL: https://link.aps.org/doi/10.1103/PhysRevB.37.9439.

Moessner, R and K S Raman (2008). "Quantum Dimer Models (Review article)". In: arXiv: arXiv:0809.3051v1.

Moessner, R. and S. L. Sondhi (2001). "Resonating valence bond phase in the triangular lattice quantum dimer model". In: *Physical Review Letters*. ISSN: 00319007. DOI: 10.1103/PhysRevLett.86.1881. arXiv: 0007378 [cond-mat].

Moessner, R., S. L. Sondhi, and P. Chandra (2000). "Two-dimensional periodic frustrated ising models in a transverse field (arXiv version)". In: *Physical Review Letters*. DOI: 10.1103/PhysRevLett.84.4457. arXiv: 9910499 [cond-mat].

Nikolic, P. and T. Senthil (2003). "Physics of low-energy singlet states of the Kagome lattice quantum Heisenberg antiferromagnet". In: *Phys. Rev. B* 68 (21), p. 214415. DOI: 10.1103/PhysRevB.68.214415. URL: https://link.aps.org/doi/10.1103/PhysRevB.68.214415.

Proust, C. and L. Taillefer (2018). "The Remarkable Underlying Ground States of Cuprate Superconductors". In: *to be published*. URL: https://arxiv.org/abs/1807.05074.

Punk, M., A. Allais, and S. Sachdev (2015). "A quantum dimer model for the pseu-dogap metal". In: ISSN: 0027-8424. DOI: 10.1073/pnas.1512206112. arXiv: 1501.00978.

Ralko, A. et al. (2005). "Zero-temperature properties of the quantum dimer model on the triangular lattice". In: *Phys. Rev. B* 71 (22), p. 224109. DOI: 10.1103/PhysRevB.71.224109. URL: https://link.aps.org/doi/10.1103/PhysRevB.71.224109.

Rokhsar, D.S. and S.A. Kivelson (1988). "Superconductivity and the quantum hard-core dimer gas". In: *Physical Review Letters*. ISSN: 00319007. DOI: 10.1103/PhysRevLett.61.2376.

Sachdev, S. and D. Chowdhury (2016). "The novel metallic states of the cuprates: Topological Fermi liquids and strange metals". In: *Progress of Theoretical and Experimental Physics*. ISSN: 20503911. DOI: 10.1093/ptep/ptw110. arXiv: 1605.03579.

Samuel, S. (1980). "The use of anticommuting variable integrals in statistical mechanics. I. The computation of partition functions". In: *Journal of Mathematical Physics* 21, pp. 2806–2814. DOI: 10.1063/1.524404.

Senthil, T. and M. P. A. Fisher (2000). "Z_2 gauge theory of electron fractionalization in strongly correlated systems". In: *Phys. Rev. B* 62 (12), pp. 7850–7881. DOI: 10.1103/PhysRevB.62.7850. URL: https://link.aps.org/doi/10.1103/PhysRevB.62.7850.

Senthil, T., Subir Sachdev, and Matthias Vojta (2003). "Fractionalized Fermi Liquids". In: *Phys. Rev. Lett.* 90 (21), p. 216403. DOI: 10.1103/PhysRevLett.90.216403. URL: https://link.aps.org/doi/10.1103/PhysRevLett.90.216403.

Sutherland, Bill (1988). "Systems with resonating-valence-bond ground states: Correlations and excitations". In: *Physical Review B*. ISSN: 01631829. DOI: 10.1103/PhysRevB.37.3786.

Zeng, C. and V. Elser (1995). "Quantum dimer calculations on the spin-1/2 kagomé Heisenberg antiferromagnet". In: *Phys. Rev. B* 51 (13), pp. 8318–8324. DOI: 10.1103/PhysRevB.51.8318. URL: https://link.aps.org/doi/10.1103/PhysRevB.51.8318.